Jin *et al. Microstructures* 2024;4:2024054
DOI: 10.20517/microstructures.2024.36

Microstructures

Review

Open Access

Construction and catalytic applications of advanced ceramic-supported single atoms

Chulong Jin, Qingqing Zhang, Adjapong Linda Akua Agyapomaa, Haiqi Zhang, Xiaojun Zeng

School of Materials Science and Engineering, Jingdezhen Ceramic University, Jingdezhen 333403, Jiangxi, China.

Correspondence to: Prof. Xiaojun Zeng, School of Materials Science and Engineering, Jingdezhen Ceramic University, Jingdezhen 333403, Jiangxi, China. E-mail: zengxiaojun@jcu.edu.cn

How to cite this article: Jin C, Zhang Q, Linda Akua Agyapomaa A, Zhang H, Zeng X. Construction and catalytic applications of advanced ceramic-supported single atoms. *Microstructures* 2024;4:2024054. https://dx.doi.org/10.20517/microstructures.2024.36

Received: 28 Apr 2024 **First Decision:** 5 Jun 2024 **Revised:** 18 Jun 2024 **Accepted:** 24 Jun 2024 **Published:** 4 Sep 2024

Academic Editor: Dingsheng Wang **Copy Editor:** Fangling Lan **Production Editor:** Fangling Lan

Abstract

In the domain of novel catalyst design and application, single-atom catalysts (SACs) have attracted widespread interest due to their ability to provide high catalytic activity and maximize the utilization of active sites. Various support materials capable of effectively anchoring single metal atoms have been reported, among which ceramic materials have received notable attention due to their distinctive versatility. This work primarily aims to elucidate the unique role of typical ceramic carriers in anchoring, isolating metal atoms, and participating in catalytic reactions. Here, we will clarify the interaction between metal atoms and ceramic carriers to explain the stabilization of atomic metal sites and the rational adjustment of individual atomic geometry and electronic structures. Furthermore, a comprehensive summary of recent research progress in SACs, with particular emphasis on advancements in preventing the migration or aggregation of isolated metal atoms, has also been stated. Regarding applications, we review the utilization of ceramic-supported SACs in electrocatalysis, photocatalysis, and other catalytic reactions. Finally, we discuss the challenges and prospects of ceramic-supported SACs in this field.

Keywords: Ceramics, single atoms, catalytic applications, stabilization, support materials

INTRODUCTION

The world is currently facing critical issues of depleting non-renewable energy sources and escalating environmental pollution, which have become urgent problems requiring immediate attention from human

society[1-3]. Transforming the pollutants generated by fossil energy into valuable commodities, such as carbon (C) dioxide reduction and nitrogen (N) reduction, offers an ideal solution pathway[4,5]. Additionally, the pursuit of clean renewable energy sources, such as electrocatalytic or photocatalytic water splitting for hydrogen production, is of paramount importance[6]. These chemical reactions have become focal points of research. Generally, appropriate catalysts are required in these conversion processes to enhance reaction rates. However, improving the catalytic performance of catalysts still poses significant challenges.

Critical to the catalytic performance of a catalyst is the consideration of factors such as size, corner positioning, and edge placement, all of which collectively determine its high specific surface area[7-10]. The size of the catalyst stands out as one of the pivotal factors influencing its overall performance. Catalytic reactions typically occur predominantly at the catalyst surface, with internal atoms playing a negligible role[11-13]. From this perspective, reducing nanoparticles to singular atoms proves to be a highly effective strategy, amplifying surface area and triggering quantum size effects[14]. As the size of nanoparticles diminishes, distinct physicochemical properties emerge, characterized by a notable increase in the count of exposed surface atoms, alongside alterations in surface atomic and electronic structures, as well as surface defects. Moreover, due to advantageous geometric and electronic effects, this increase significantly enhances the density of active sites, correspondingly enhancing intrinsic activity, an essential aspect in achieving unconventional catalytic performance[15-18]. In this regard, Qiao *et al.* pioneered the fabrication of the first successful Pt single-atom catalyst and introduced the concept of single-atom catalysts" (SACs), defined as supported metal catalysts housing exclusively isolated single metal active sites on the surface[19]. Consequently, owing to their maximal atomic utilization efficiency, unsaturated active sites, and clear reaction mechanisms, SACs have emerged as one of the leading catalyst systems to date[20]. However, despite the dispersion method of single atoms (SAs) theoretically enabling 100% atomic utilization as nanoparticle size diminishes, surface energy escalates significantly, leading to metal atom aggregation, as shown in Figure 1A and B[21,22]. Therefore, the judicious selection of suitable support materials to anchor singly dispersed metal atoms has become indispensable in stabilizing these metal atoms and advancing single-atom catalysis[23].

Currently, various support materials required for SACs have garnered widespread research interest[24]. Due to the high surface-to-volume ratio of single metal atoms, they can strongly interact with oxides[25-27], carbon-based materials[28-30], ceramics[31], and metal-organic frameworks (MOFs)[32], facilitating effective dispersion of metal atoms and preventing agglomeration phenomena. Such intense interactions may lead to dynamic charge transfer at the interface, thereby influencing the catalytic performance of SACs. Although porous MOFs with high surface areas are considered promising support materials for anchoring SACs, the structural instability of the pristine MOFs limits their application in electrochemical applications[33]. Compared with other materials, ceramic materials are more attractive in catalytic applications due to their higher stability at high temperatures[34]. Ceramic materials also possess specific and variable properties. For example, the abundant defect sites (steps, vacancies) and -OH groups on the surface can serve as anchor sites for single metal atoms[25]. Furthermore, through chemical modification, metal-support interactions can be established, and this synergistic effect greatly affects catalytic performance. The robustness of oxides at high temperatures is also an important factor in enhancing the mechanical and thermal stability of SACs. Therefore, among various supported SACs, ceramic-supported SACs are particularly interesting. Ceramic-supported SACs are particularly intriguing among the numerous supported SACs due to their diverse properties in various ceramic materials, including high-temperature stability and the presence of abundant coordinatively unsaturated sites on the surface[35,36].

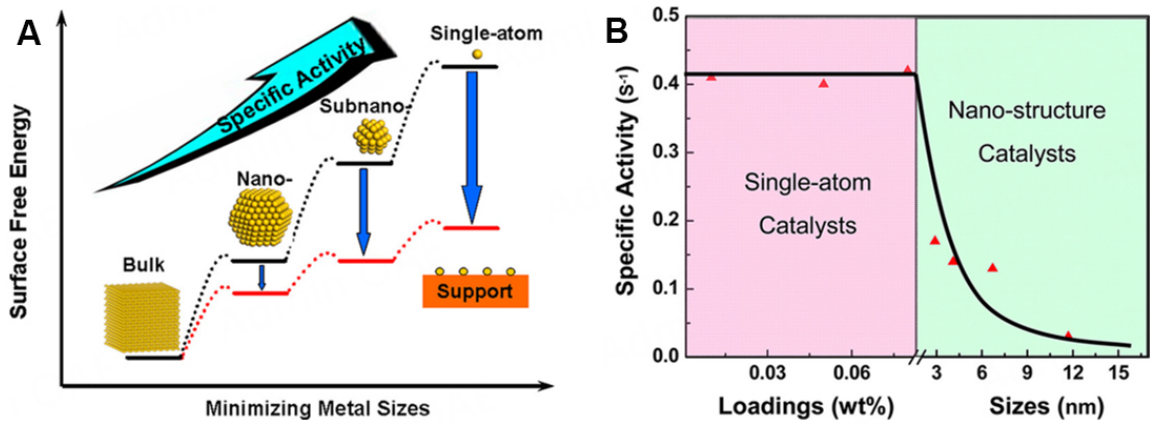

Figure 1. (A) Relationship between size and reactivity of nanomaterials[21]. (B) Specific activity as a function of metal loading and size[22].

This paper presents a comprehensive overview of research on SACs supported by ceramics in the field of energy conversion. The performance of SACs is intricately linked to their geometric and electronic structures. Therefore, we have selected representative and recent cases, including oxides, perovskites, spinels, MXenes, and other ceramic-based SACs, and delved deeply into the structure-property relationships among them. Additionally, we emphasize the analysis of interactions between single metal atoms and ceramic supports. Furthermore, we discuss several pivotal catalytic reactions (oxygen evolution (OER), hydrogen evolution (HER), oxygen reduction (ORR), carbon dioxide reduction (CO_2RR), nitrogen reduction (NRR), and carbon dioxide hydrogenation reactions (CO_2HR)), alongside pertinent theoretical investigations and reaction mechanisms, as detailed in Figure 2. We aim to provide valuable insights for exploring potential ceramics for SACs. The final section provides a concise summary and outlook on the development of ceramic-supported SACs, elucidating potential challenges and outlining future research directions.

DIFFERENT TYPES OF CERAMIC-SUPPORTED SACS

In the field of energy conversion catalysts, various types of SACs exhibit unique characteristics. Through careful selection of supports, we can manipulate the spatial configuration and coordination environment of single metal atoms in different carriers, thereby enhancing catalytic performance. This section focuses on the catalytic activity of single metal atoms on various ceramic supports. Firstly, we focus on oxides such as Al_2O_3, ZrO_2, and CeO_2, as they are among the most widely used supports. Subsequently, we investigate spinel, characterized by exceptional chemical and thermal stability, along with tunable pore structures and surface active sites, rendering them ideal catalytic carriers capable of facilitating efficient reaction environments across diverse conditions. Following that, we present perovskites as structurally stable materials proficient in securely anchoring SACs loaded on their surfaces, thus averting aggregation and deactivation, consequently augmenting catalyst stability and recyclability. Finally, we discuss the application prospects of MXene as a novel class of two-dimensional materials. MXene has abundant surface functional groups and active sites, and by loading SACs on its surface, active metal atoms can be effectively dispersed and anchored on the carrier, thereby improving the stability and activity of the catalyst. SACs demonstrate enormous potential in the field of catalysis, being widely applied not only in electrocatalysis[37] and photocatalysis[38], but also garnering extensive attention in the battery domain[39,40].

Typical oxide carriers

Oxide supports emerge as an ideal choice for metal catalysts due to their high surface area and diverse defect

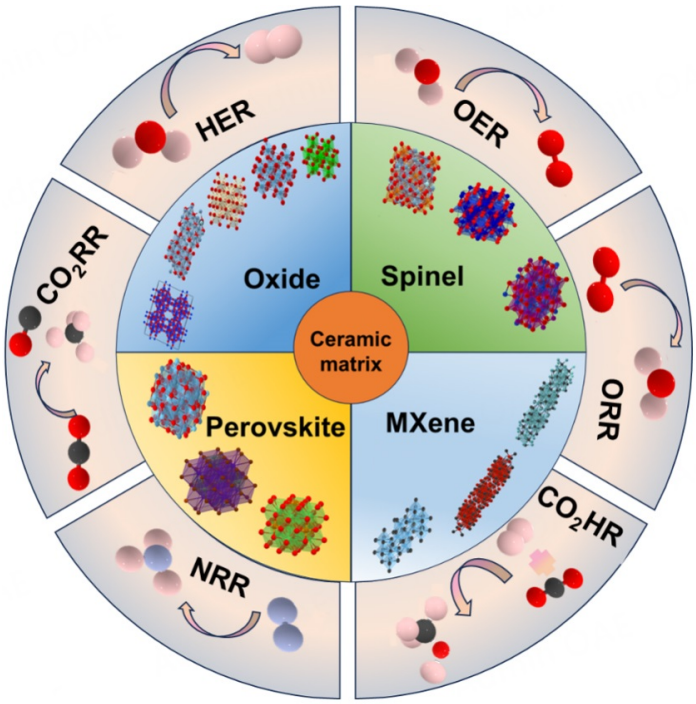

Figure 2. Typical ceramic supports and their catalytic applications.

types, such as oxygen vacancies (O_v), metal vacancies (M_v), edges, and steps. These defects are considered ideal anchoring sites for single-atom metals since they can be tailored through the crystal structure and synthesis conditions of oxides, thereby influencing the adsorption and stability of single-atom metals[41-44]. In the absence of reducing conditions, according to the Toppolin electron rule, positively charged single-atom metals can stably adsorb onto surface bonds M-O(H) with a slight negative charge[45]. Oxides such as CeO_2, TiO_2, Al_2O_3, SiO_2, and ZrO_2 exhibit advantages in immobilizing individual metal atoms, not only stabilizing them but also participating in reactions, where surface cations of oxide supports can be replaced by metal atoms, interacting with adjacent oxygen anions to further enhance stability. These characteristics render oxide supports highly valuable in supporting SACs, enhancing catalyst stability and activity, thus playing a pivotal role in the catalysis domain.

CeO_2-supported SACs

CeO_2 stands as a pivotal 4f oxide; thanks to continuous optimization of its manufacturing process, it increasingly meets the requirements for large-scale production. It has garnered extensive attention and research across a range of applications including electrocatalysis, biosciences, and electronic ceramics[46-48]. Due to its unique properties, it is widely used as a support material for SACs. Known for its high density of vacancies and reversible oxygen storage process, CeO_2 enables the modulation of local coordination environments and electronic states of metal atomic sites in SACs through redox thermal activation. During oxidative calcination, the metal nanocrystalline structure on the CeO_2 support can form covalent M-O bonds, facilitating the dispersion of metal atoms at the atomic scale[49,50]. Notably, CeO_2 has also garnered attention for its strong metal-support interaction (SMSI) with noble metals, enabling the stable existence of noble metals in highly dispersed forms[51,52]. Strategies such as low metal loading, high surface area nanoscale carriers, or a combination of both are commonly employed to prevent the aggregation of active phases in noble metal SACs. Additionally, nanoscale structures can significantly alter the chemical properties of CeO_2[53-56]. Wang *et al.* demonstrated an optimized method for CO_2 electrocatalytic reduction to methane

(CH_4) through atomic design, replacing CeO_2 with single-atom copper combined with multiple O_v[57]. Theoretical calculations predict that single-atom copper substitution can enrich up to three O_v on the CeO_2 surface, enhancing CO_2 adsorption and activation, as shown in Figure 3A. Experimental verification confirmed the effectiveness of this design, revealing the highly dispersed single-atom copper in CeO_2 nanorods [Figure 3B], directly correlated with O_v. This catalyst design exhibited up to 58% Faradaic efficiency (FE), indicating its outstanding activity and selectivity in converting CO_2 to CH_4, offering a new atomic-level solution in this field. These findings not only elucidate the role of CeO_2 in SACs but also provide crucial guidance for the design and application of future catalysts. Xu *et al.* successfully synthesized highly active and durable Rh SACs using a "wrap-bake-peel" technique, addressing both poor activity and stability issues, as shown in Figure 3C[58]. In the synthesis process of the catalyst, the pre-coated SiO_2 layer not only protects the CeO_2 support from sintering but also provides electrons to weaken the Ce-O bonds, thus promoting the formation of highly loaded Rh SAs on the CeO_2 support.

TiO_2-supported SACs

Within natural environments, TiO_2 manifests in three principal crystalline forms: rutile, anatase, and brookite. Rutile stands as the most stable phase, while anatase and brookite may transition to rutile under thermal treatments. Due to its abundant raw materials and cost-effective production, TiO_2 has become a prominent material in various emerging research domains, including energy conversion and storage, environmental remediation, and optoelectronics[59]. Notably, TiO_2 in rutile and anatase phases finds extensive application as catalyst support due to its indispensable roles in catalytic reactions[60]. Throughout catalysis, the migration of metal atoms facilitates the emergence of O_v and Ti^{3+} sites on TiO_2 surfaces, thereby fostering the development of active metal-TiO_2 interfaces[61-63]. Wan *et al.* proposed a methodology to stabilize single-atom sites through the introduction of defects on the support surface, resulting in the fabrication of nanosheets with exceptional catalytic performance by supporting single-atom Au on defective TiO_2, as shown in Figure 4A and B[64]. These defects serve to diminish energy barriers and mitigate competitive adsorption among isolated Au atomic sites, thus amplifying catalytic efficiency. And the elements are evenly distributed [Figure 4C]. Yang *et al.* introduced a novel strategy to stabilize isolated gold atoms via ultraviolet (UV) irradiation of titanium dioxide supports, achieving stabilization in ethanol[65]. This method facilitates the facile dissociation of water molecules on gold-oxygen-titanium dioxide sites, ensuring that even nanoscale particles formed at elevated gold loadings do not augment the activity of gold-bound atoms on titanium dioxide. The integrity of the catalytic activity is upheld by eliminating excess gold through sodium cyanide leaching, thereby ensuring the steadfast binding of atomically dispersed gold to titanium dioxide. These investigations underscore the potential of defect engineering in optimizing catalyst performance, thereby furnishing novel pathways for the design of efficacious catalysts.

Al_2O_3-supported SACs

Al_2O_3 plays a pivotal role in industrial catalysis. Thanks to advanced production technology and abundant raw materials, it is cost-effective and widely used in refractory and electronic components[66-69], particularly as a carrier for metal catalysts. Despite the lack of covalent metal-support bonds, Al_2O_3 can stabilize individual metal atoms on its surface through metal-oxygen/hydroxyl interactions[70,71]. This stability allows the metal species to connect with the porous nanostructure supported by Al_2O_3, maintaining the dispersion of metals[72]. This strategy not only aids in enhancing the activity and stability of catalysts but may also influence surface properties such as surface charge transfer, changes in metal structure, and regulation of molecular adsorption, thereby affecting catalyst performance[73-75]. However, due to the relatively weak metal-support interaction of Al_2O_3 for stabilizing isolated active metal atoms, further modification of the support cations may be necessary to achieve better performance. Mesoporous alumina presents a feasible option due to its increased defect sites, which can enhance the interaction between metal and support,

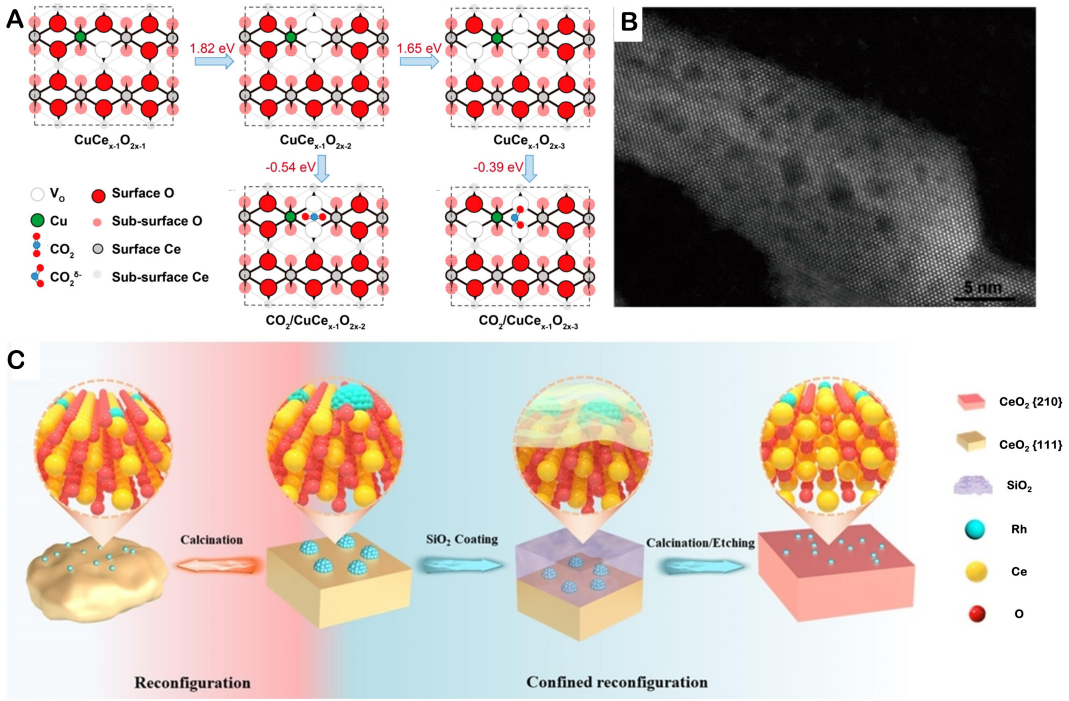

Figure 3. (A) Theoretical calculations of the most stable structures of Cu-doped CeO_2(110) and their effects on CO_2 activation. (B) HRTEM images of Cu-CeO_2-4% nanorods[57]. (C) Schematic illustration of "wrap-bake-peel" synthetic strategy[58].

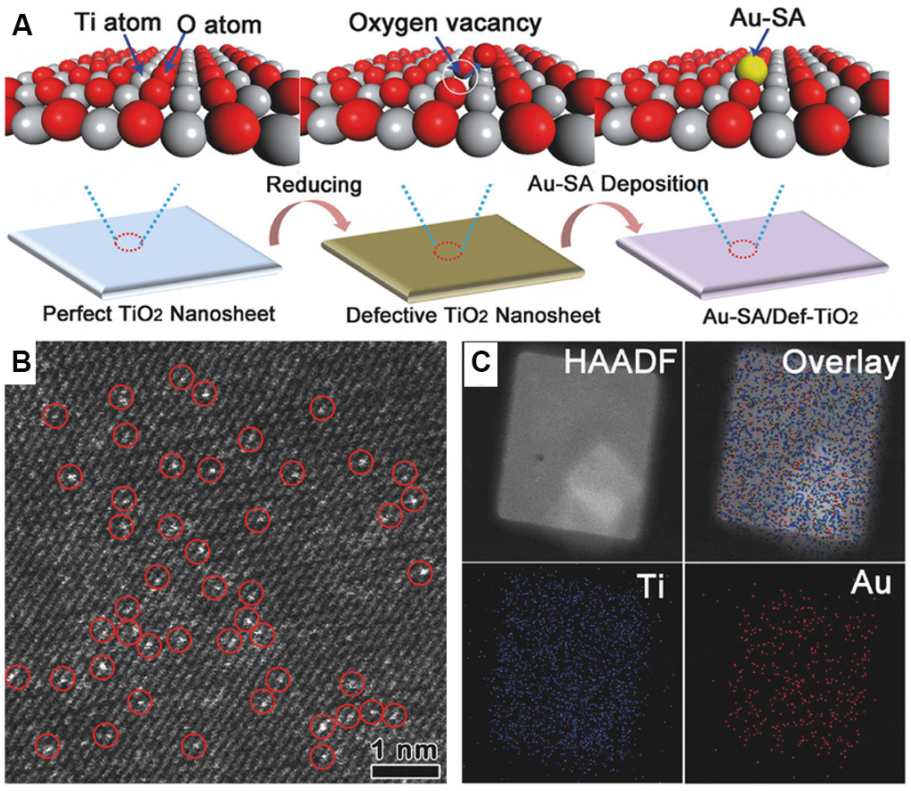

Figure 4. (A) Schematic illustration of synthesis procedure and the results of Au-SA/Def-TiO_2. (B) HAADF-STEM image, single atomic Au sites highlighted by red circles. (C) Elemental mappings show the distribution of Ti (blue) and Au (red)[64].

further improving catalytic performance[76,77]. Shang *et al.* successfully prepared atomically dispersed platinum nanosheets (Pt/dp-Al_2O_3) on mesoporous alumina support using a combination of wetness and thermal decomposition methods[78], as shown in Figure 5A. These nanosheets exhibited high-density active sites, strong anchoring effects and interfacial synergy between the support and platinum atoms. Zhang *et al.* also described a highly stable, atomically dispersed Pt catalyst supported on mesoporous Al_2O_3[79]. The catalyst was synthesized using an enhanced sol-gel solvent evaporation self-assembly approach, followed by calcination in air and then reduction with H_2, as shown in Figure 5B. Owing to the stability of the coordinatively unsaturated tetrahedral Al^{3+} centers, Pt atoms were securely immobilized on the inner surface of mesoporous Al_2O_3. This catalyst retained its catalytic activity and structural integrity throughout a series of prolonged, rigorous reactions.

SiO_2-supported SACs

SiO_2 has abundant reserves on Earth and has become an indispensable material in various fields such as catalysis and biotechnology[80-83]. Similar to Al_2O_3, SiO_2 is also an irreducible oxide. It has been reported that various metals such as Pt[84] can be atomically dispersed on SiO_2 and utilized in catalytic reactions such as catalytic cracking, epoxidation, methanol carbonylation, and C-H bond functionalization[85-88]. However, under reaction conditions, metals initially deposited or grafted onto the SiO_2 surface often tend to aggregate. To address this issue, several strategies have been developed, such as incorporating alkali ions (Na^+, K^+) or ligands containing nitrogen during synthesis[89,90]. Zhai *et al.* found that adding metals to silica surfaces promoted by alkali ions has a similar effect to adding metals to ceria[91]; that is, the surface oxygen associated with metals and alkali ions becomes reducible at low temperatures, and the presence of alkalis during heat treatment inhibits the growth of metal particles. This indicates that Na-modified silica-supported Pt atoms remain stable after heat treatment. Nevertheless, a more effective approach is to confine metal species within the supporting lattice or even immobilize them within porous solid materials. For example, hydrated metal aluminosilicate compounds, namely zeolites, can form three-dimensional channel structures. Zeolites greatly enhance the thermal stability of isolated metal atoms, as the framework cavities within zeolites act as traps preventing further aggregation via the Brownian motion of metal atoms. Transition metals (TMs) can be easily loaded into zeolites via ion exchange methods, with framework oxygens in the ring pockets stabilizing the metal atoms. Additionally, depending on the pore size and shape, molecular sieves are commonly employed for molecular separations. Thus, using zeolites as catalyst supports can be expected to enhance the activity and/or selectivity of the catalyst[92]. Li *et al.* proposed a novel strategy involving the grafting of separated and defective CeO_x nanoclusters onto high-surface-area SiO_2, wherein each nanocluster hosts an average of one platinum atom[93]. This involved the grafting of separated and defective CeO_x nanoclusters onto high-surface-area SiO_2, wherein each nanocluster hosts an average of one platinum atom. They observed that Pt atoms remained dispersed even under high-temperature oxidation and reduction conditions, resulting in a significant enhancement in the CO oxidation activity of the catalyst. This approach ensures the mobility of Pt atoms while constraining them within their respective nanoclusters. The utilization of functional nanoclusters to confine metal atom dispersion and concurrently enhance reactivity represents a prevalent strategy, thereby bridging the gap between SACs and practical applications.

ZrO_2-supported SACs

ZrO_2 commonly exists in multiple crystal forms, each exhibiting distinct physical properties[94]. ZrO_2 ceramics are renowned for their excellent thermal and chemical stability and have been widely used in various fields, such as solid oxide fuel cells, biomedical sectors, and high-temperature structural ceramics[95-97]. Notably, in the monoclinic crystal system of ZrO_2, there is a higher concentration of hydroxyl groups, facilitating the binding of individual metal atoms and thus presenting significant advantages in the

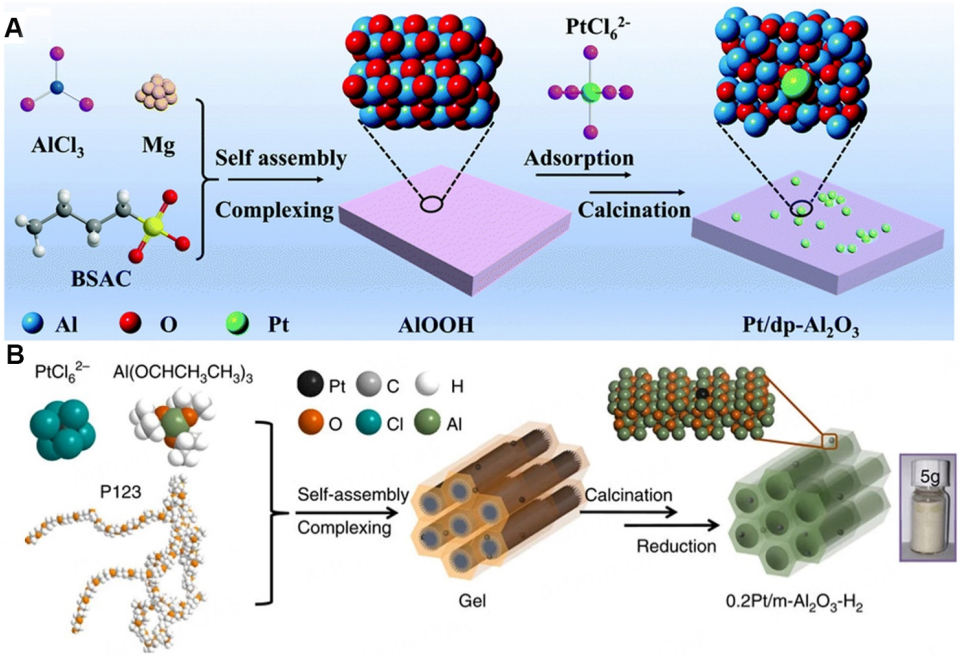

Figure 5. (A) Schematic illustration of the formation of Pt/dp-Al_2O_3[78]. (B) Schematic illustration of the 0.2Pt/m-Al_2O_3-H_2 synthesis process[79].

field of single-atom catalysis[98,99]. The surface of zirconia possesses abundant active sites capable of securely anchoring individual metal atoms, thereby providing reliable active centers for catalytic reactions[100,101]. Additionally, the electronic structure of zirconia can be modulated through the control of surface oxidation states and lattice defects, optimizing the catalytic performance and selectivity of SACs. The zirconia surface exhibits excellent resistance to poisoning, reducing the risk of catalyst impairment by external impurities and toxic substances, thus enhancing its long-term stability and catalytic activity[102,103]. Zirconia SACs have demonstrated broad application prospects in fields such as redox reactions and hydrocarbon conversion[104]. Du *et al.* successfully immobilized Nb SAs onto a ZrO_2 substrate (Nb_1-ZrO_2)[105]. Their study revealed that the formation of Nb_1-Zr dual sites on Nb1-ZrO_2 enhanced the adsorption and activation of NO_2, optimized the adsorption of key ammonia (NH_3) intermediates, and decreased the reaction energy barrier, leading to an improvement in the activity of NO_2RR. Choudhary *et al.* utilized an easy co-precipitation method to produce Co/ZrO_2 SACs[106]. Their study revealed that cobalt-doped ZrO_2 acts as a SAC, with each Co^{2+} ion facilitating CO_2 fixation. Characterization of the Co/ZrO_2 catalyst through EXAFS and STEM affirmed the existence of isolated Co^{2+} species on the ZrO_2 support.

Spinel-based carriers

Spinel is a category of materials possessing a unique crystal structure, with a general chemical formula of AB_2O_4, where A and B represent two different metal ions, and X denotes oxygen ions. Spinel exhibits remarkable activity and high stability owing to its typical crystal structure[107], and holds important promise for applications in cutting-edge domains, especially in battery technology and electromagnetic wave absorption materials[108-110]. In AB_2O_4, TM cations occupy octahedral sites (TMoct) consisting of six oxygen anions and tetrahedral sites (TMtd) composed of four oxygen anions, with TMoct typically serving as the primary active sites for OER, exposed near the surface of AB_2O_4[111,112]. In a typical inverse spinel structure, all A^{2+} cations and half of the B^{3+} cations occupy TMoct, facilitating electron transitions between A^{2+} and B^{3+}, achieving higher conductivity, and providing more surface redox-active centers from A^{2+} and B^{3+} with different oxidation states, thereby accelerating reaction kinetics[113,114]. Due to the typical lattice structure of

AB_2O_4, oxygen anions are shared by one TMtd and three TMoct, reducing electron polarization from oxygen anions to TM cations between neighboring cations, decreasing overlap between metal-d and oxygen-p orbitals, thereby suppressing the covalency of TM-O bonds[115,116]. Therefore, spinel, as a crystal material with unique structure and properties, holds broad application prospects in energy conversion and storage applications[117]. Its low cost, accessibility, high activity, and stable catalytic properties provide important support for the design and development of efficient and stable SACs. Shan *et al.* designed a catalyst by placing iridium SAs on the cationic sites of cobalt oxide spinel, synthesizing $Ir_{0.06}Co_{2.94}O_4$, as shown in Figure 6A[118]. This catalyst exhibited twice the oxygen evolution performance of cobalt oxide under acidic conditions. Due to the strong interaction between iridium and the cobalt oxide support, the corrosion resistance and oxidation potential of $Ir_{0.06}Co_{2.94}O_4$ catalyst significantly improved under acidic conditions. This work eliminates the "close-packing" limitation of noble metals and provides promising opportunities for creating analogs with diverse catalytic applications requiring specific topological structures. Wang *et al.* introduced an innovative approach involving single-atom bismuth (Bi) doping, resulting in the synthesis of single-atom dual-doped Co_3O_4 (Bi-Co_3O_4) through a combination of electrodeposition and calcination techniques, as shown in Figure 6B[119]. Experimental characterization alongside theoretical computations unveiled that single Bi atoms replaced cobalt ions at the octahedral positions within the Co_3O_4 structure, thereby facilitating the generation of active hydroxyl groups at nearby tetrahedral Co sites. This study highlights the promising avenue of employing single-atom doping strategies to enhance the electrocatalytic performance of spinel oxides.

Perovskite-based carriers

Perovskite oxides have garnered significant attention due to their outstanding high-temperature stability and pristine ABO_3 crystal structure[120-122]. Perovskite materials have attracted great attention due to their excellent photoelectric properties and impressive conversion rates, particularly in the field of optoelectronic sector[123,124]. Firstly, their exceptional lattice and chemical stability ensure reliable surface support, aiding in the preservation of individual metal atom stability and the formation of stable surface active sites crucial for catalytic reactions. These sites play a pivotal role in catalysis, effectively facilitating catalytic activity[125]. Secondly, interactions between perovskite and single metal atoms can modulate the mechanisms and activity of catalytic reactions, influencing reaction selectivity and efficiency by adjusting electronic structures, and thereby optimizing catalytic performance[126]. Furthermore, perovskite possesses a diverse electronic structure capable of charge transfer and interaction, enabling controlled modulation of catalytic activity to meet the varied demands of different catalytic reactions[127]. Its high specific surface area and abundant active sites provide ample reaction sites for catalysis, while defects in the lattice and surface O_v further enhance catalytic performance[128]. Lastly, perovskite not only serves as a carrier for SACs but also, through structural and compositional adjustments, achieves multifunctional regulation of various catalytic reactions, exhibiting extensive application prospects[129-131]. Tian *et al.* first reported the loading of single metal atoms onto perovskite oxides, utilizing heterostructure perovskite as a unique nanostructure for SAC immobilization[132]. The authors provided a generalizable method for manufacturing highly stable Au monoatomic catalysts with tunable catalytic properties. The resulting Au SAC not only exhibits resistance to sintering at 700 °C but also demonstrates high catalytic activity under reaction conditions, displaying significant self-activation activity. This discovery has significantly spurred the exploration of other perovskite-loaded metal SACs, thereby advancing their catalytic applications. Shin *et al.* introduced a versatile method for fabricating SACs on metal, metal oxide, and perovskite nanosheet scaffolds[133]. They achieved an impressive metal loading of up to 3.94 wt% by utilizing nitrogen-doped graphene as a sacrificial template to confine SAs spatially. Initially, the research team anchored the precursor of the target support material onto the stable sacrificial template hosting SAs. Subsequent thermal treatment facilitated the transfer of SAs onto the support material while eliminating the graphene layer, as shown in Figure 7. Remarkably, Pt SAs on the oxide carrier displayed minimal aggregation during annealing at temperatures

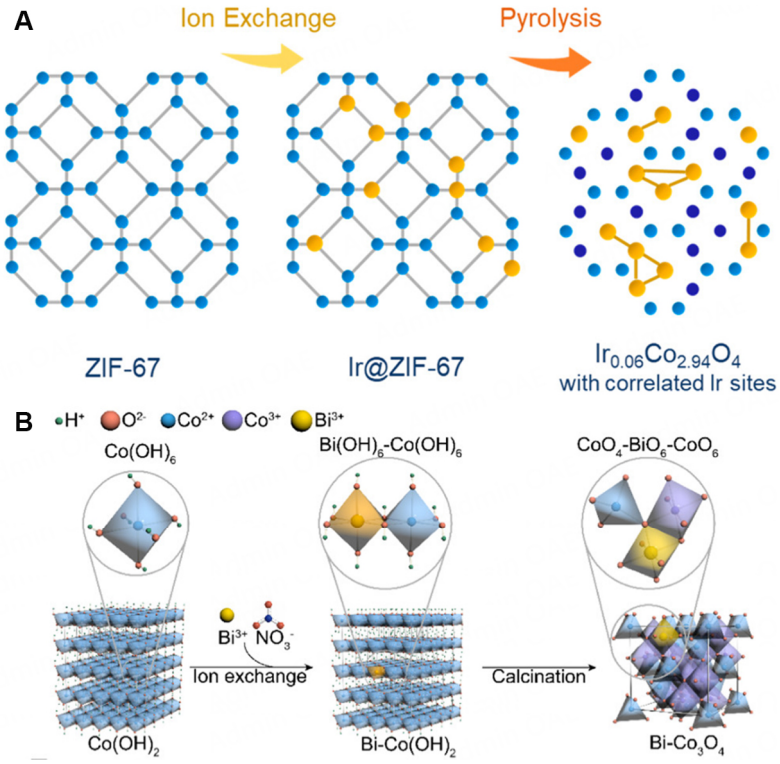

Figure 6. (A) Synthesis Schematic of $Ir_{0.06}Co_{2.94}O_4$ [118]. (B) Schematic illustration of the synthesis strategy for single-atom Bi-doped Co_3O_4 catalyst[119].

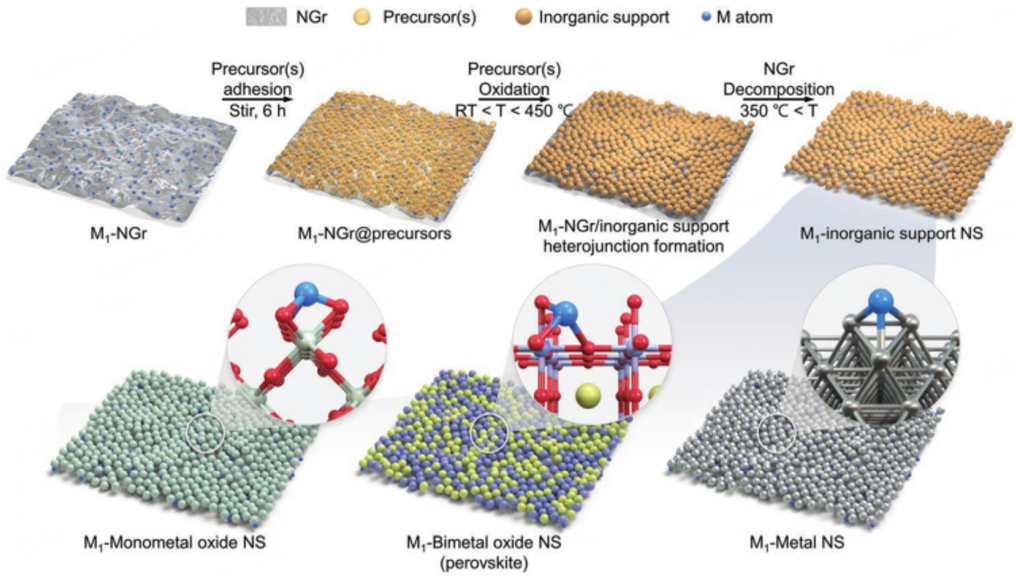

Figure 7. Schematic illustration for the synthesis of Pt single-atoms stabilized on various inorganic (metal oxide, perovskite, and metallic) nanosheets via the N-doped graphene sacrificial templating route[133].

exceeding 275 °C for over 10,000 min, highlighting their outstanding thermal stability. Therefore, perovskites exhibit enormous potential in stabilizing SAs at high temperatures.

MXene-based carriers

In recent years, researchers have drawn attention to the exceptional capability of two-dimensional materials to effectively stabilize individual metal atoms[134]. The inherent thin-layered structure of these materials provides a larger surface area and numerous anchoring points, facilitating the synthesis of SACs with high loadings. Among these materials, MXenes have emerged as a novel and innovative class of two-dimensional materials characterized by their surface terminal groups[135], offering the potential to serve as support for anchoring atomic metal species. They have garnered widespread interest across various disciplines due to their unique surface chemistry, graphene-like morphology, metallic conductivity, high hydrophilicity, excellent mechanical properties, and redox capabilities, leading to rapid advancements and applications in fields such as electrochemistry, catalysis, and photothermal conversion[136-139]. Notably, MXene sheets typically exhibit spontaneously formed M_v during synthesis, offering advantages for the introduction and modification of heteroatoms[140]. What sets MXenes apart from other two-dimensional materials is their exceptional tunability in terms of electronic bandgaps, conductivity, and charge transfer rates. The monolayer structure of MXenes, characterized by hexagonal symmetry akin to graphene, adopts an interlayer structure with X as the central layer and M as the edge layer. It is coordinated by six N or C atoms directly with M and surrounded by a series of surface terminal functional groups and metal coordination. Some MXenes are more prone to decompose into monolayer structures, which can be achieved by adjusting the elemental ratios of M and X to tailor the material's structure and properties, or by modifying terminal functional groups to enhance material characteristics such as hydrophilicity/hydrophobicity, conductivity, and stability. The controlled formation of defect sites during synthesis renders MXenes an ideal support material for the fabrication of SACs[141-144]. Furthermore, through the modulation of the central metal type and substitution of terminal groups with other functional groups, the electronic bandgap width of MXenes can be readily adjusted, a feat challenging to achieve with other two-dimensional materials such as graphene[145,146]. Ramalingam *et al.* demonstrated the synthesis of isolated ruthenium SAs (Ru_{SA}) and $Ti_3C_2T_x$ MXene supported by N and sulfur (S) heteroatom-doped carriers, as shown in Figure 8A[147]. The stabilization of Ru_{SA} on the MXene carrier was facilitated through Ru-N and Ru-S bonds formed with N and S atoms, respectively. The coordinated species of N and S in Ru_{SA}-N-S-$Ti_3C_2T_x$ significantly enhanced the catalytic activity of HER in acidic solutions. Additionally, Zhang *et al.* introduced Pt SAs (Pt_{SA}) onto monolayer $Ti_3C_2T_x$ matrices using a rapid thermal shock strategy under H_2 atmosphere, exploiting unconventional methods due to the formation of O_v in hydroxylated MXenes during conventional annealing in H_2, as shown in Figure 8B[148]. Post-H_2 annealing of monolayer $Ti_3C_2T_x$ was shown to induce O_v formation under reducing atmospheres. High-angle annular dark-field scanning transmission electron microscopy (HAADF-STEM) and density functional theory (DFT) calculations confirmed that O_v formation on monolayer $Ti_3C_2T_x$ could be captured through Pt-Ti bonding to trap Pt_{SA}.

CATALYTIC APPLICATION OF CERAMIC-SUPPORTED SINGLE ATOM

SACs have gained widespread application in catalytic fields such as thermal catalysis, electrocatalysis, and photocatalysis due to their unique structure, which exhibits distinct properties from nanoparticle catalysts. In this section, we will focus on the applications of SACs in various catalytic reactions, including OER, HER, ORR, CO_2RR, NRR, and CO_2HR, as shown in Table 1. We will conduct detailed investigations into the mechanisms and structure-performance relationships of these reactions from both experimental and theoretical perspectives.

Electrocatalytic application

With the rapid increase in the production of sustainable and renewable energy sources, there is a growing emphasis on electrochemical performance[149,150]. However, limitations still exist in the catalytic performance required for various electrocatalytic systems. Therefore, efforts are being made to find more rational approaches, such as controlling the size, shape, composition, and structure of electrocatalysts, to enhance

Table 1. Catalytic application of ceramic-based SACs

Catalyst	Atomic species	Carrier type	Electrolytes	Application	Refs.
Pt_{SA}-Mn_3O_4	Pt	Spinel	1 M KOH	HER	[154]
Ru-ZrO_{2-x}/C	Ru	Oxide	0.5 M H_2SO_4	HER	[155]
Ir@Sr-p-TiO_2 NWs	Sr	Oxide	0.5 M H_2SO_4	OER	[162]
$Ir_1/Ni_{1.6}Mn_{1.4}O_4$	Ir	Spinel	1 M KOH	OER	[163]
Fe@ZrO_2/NC	Fe	Oxide	0.1 M KOH	ORR	[168]
Fe-N-C/$Nb_4C_3T_x$	Fe	MXene	0.1 M KOH	ORR	[169]
$Fe_{SAs+NPs}Ce_{SAs+Fe\text{-}ONPs}$/NC	Fe	Oxide	0.1 M KOH	ORR	[170]
Ru-NS-$Ti_3C_2O_2$	Ru	MXene	-	CO_2RR	[171]
$CuSiO_x$	Cu	Oxide	0.1 M $KHCO_3$	CO_2RR	[172]
Ga_{SA}/a-TiO_2	Ga	Oxide	0.1 M Na_2SO_4	NRR	[175]
LaFeO-Ru	Ru	Perovskite	0.1 M K_2SO_4	NRR	[176]
Pt_{SA}/TiO_2	Pt	Oxide	0.1 M Na_2SO_4	HER	[186]
Cu/TiO_2	Cu	Oxide	25% methanol	HER	[187]
Co-$Ti_3C_2T_x$	Co	Oxide	H_2O/acetonitrile	CO_2RR	[188]
Co-N-C@$BiFeO_3$	Co	Perovskite	-	CO_2RR	[189]
Au/Al_2O_3	Au	Oxide	H_2O	CO_2RR	[192]
Cu/ZrO_2	Cu	Oxide	-	CO_2HR	[196]
ZrO_2/Cu	Cu	Oxide	-	CO_2HR	[197]
Cu/Mo_2CT_x	Cu	MXene	-	CO_2HR	[198]

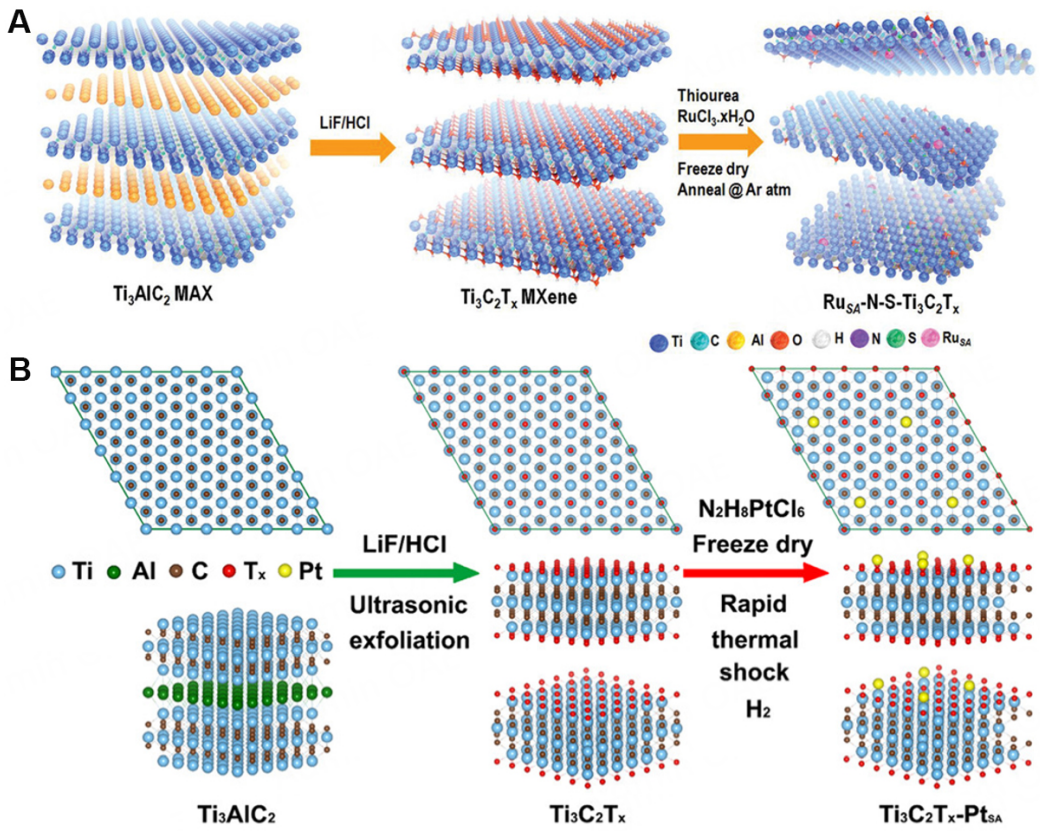

Figure 8. (A) Schematic illustration of the Ru_{SA}-N-S-$Ti_3C_2T_x$ catalyst. synthetic route[147]. (B) Schematic illustration of constructing Pt single atoms on monolayer $Ti_3C_2T_x$ [148].

catalytic efficiency[151,152]. In particular, research on SACs has sparked emerging interest in electrocatalysis due to their high catalytic activity, stability, selectivity, and 100% atom utilization. Ceramic-supported SACs exhibit great potential in electrocatalytic HER, OER, ORR, CO_2RR, and NRR, as shown in Table 1.

HER

Hydrogen is considered an ideal clean energy source, and electrocatalytic water splitting is deemed a sustainable means of production. Presently, Pt-based catalysts are recognized for their superior performance in the HER. However, the high cost associated with Pt, stemming from its limited natural abundance, poses a significant barrier to its widespread adoption. Hence, there is a pressing need to minimize Pt usage or explore alternative materials. SACs have emerged as a promising avenue, offering maximal atomic efficiency, and have, therefore, garnered significant research attention[153].

In a pioneering study, Wei *et al.* reported, for the first time, the synthesis of spinel-type Mn_3O_4-supported Pt SAC (Pt_{SA}-Mn_3O_4)[154]. This provides a reference for tuning the electronic structure of spinel oxide to obtain SAC systems with high alkaline HER activity. They unveiled the synthesis of Pt SACs supported on spinel Mn_3O_4, with Pt atoms intricately positioned at octahedral sites. The profound interaction between Pt and Mn_3O_4 significantly reshapes the electronic structure, thereby optimizing the binding strength of d-band centers and intermediates. Remarkably, under alkaline conditions, this catalyst exhibits exceptional performance in HER, showcasing an ultra-low overpotential of 24 mV at 10 mA cm^{-2} and a superior mass activity of 374 mA mg^{-1} [Figure 9A and B], eclipsing both 20 wt% Pt/C and the majority of previously reported high-performance catalysts. In investigating the adsorption capacity of catalysts for H_2O, it was observed that Pt_{SA}-Mn_3O_4 exhibited the highest adsorption capability. Additionally, the study results indicated that Pt_{SA}-Mn_3O_4 possessed the optimal water dissociation energy barrier. Graphs depict the hydrogen adsorption free energy (ΔG_{H^*}) values of single Pt atomic sites on Pt_{SA}-Mn_3O_4, which are comparable to the adsorption ΔG_{H^*} values on Pt (111) surfaces [Figure 9C and D]. This suggests that incorporating single Pt atoms into Mn_3O_4 effectively enhances the occupation of d-bands near the Fermi level of the catalyst, thereby facilitating the adsorption and dissociation processes of H_2O and H*, consequently enhancing the catalytic activity of HER under alkaline conditions.

Kim *et al.* proposed a novel approach to SACs by tightly integrating stable metal oxide nanoparticles, resulting in a significant enhancement in the electrochemical activity and stability of catalysts for HER[155]. In their study, Ru-ZrO_{2-x}/C exhibited a remarkable improvement in HER activity, particularly at high current densities, with the smallest overpotential observed when the current density exceeded 50 mA·cm^{-2}, displaying an overpotential of 19 mV lower than that of Pt/C [Figure 9E]. This enhancement is possibly attributed to the hydrophilicity of the ZrO_2 surface[156]. The formation of Ru-ZrO_2-SACs is facilitated by the generation of O_v in tetragonal ZrO_2. Additionally, after activity decay test (ADT), the overpotential of Pt/C and Ru/C increased significantly, attributed to the severe aggregation of metal particles on the carbon carrier. In contrast, the overpotential increase of Ru-ZrO_{2-x} is minimized, owing to the SMSI between Ru atoms and ZrO_2, achieving outstanding durability [Figure 9F]. When the research team sought to identify the sources of enhanced HER activity, they obtained the hydrogen adsorption energies (ΔE_{ads}) of the prepared catalysts through DFT calculations. The research findings indicate that compared to Ru (-0.50 eV) and Pt (-0.38 eV), Ru SAs on the surface of ZrO_2 exhibit more favorable ΔE_{ads} values (-0.15 eV). This suggests that Ru SACs on the ZrO_2 surface may be more conducive to promoting hydrogen adsorption and HER activity [Figure 9G].

OER

The process of water electrolysis encompasses both the HER and OER. The sluggish, multi-step proton-

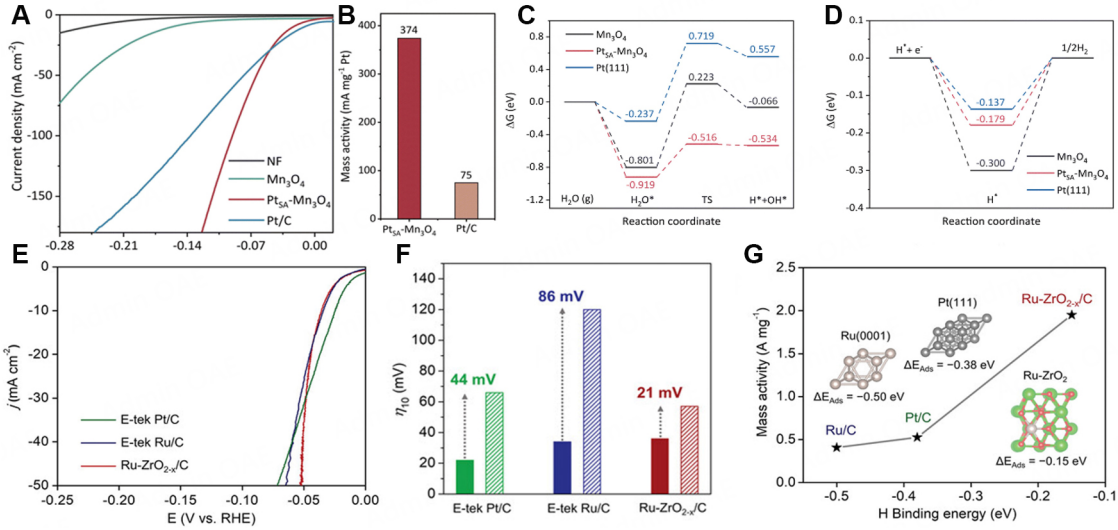

Figure 9. (A) HER polarization curves of NF, Mn_3O_4, Pt_{SA}-Mn_3O_4, and Pt/C. (B) The mass activity of Pt SA-Mn_3O_4 and Pt/C. (C and D) Calculated Gibbs free energy for the Volmer step on the surfaces, and G_{H^*} values of hydrogen evolution at the equilibrium potential of Mn_3O_4, Pt (111) and Pt_{SA}-Mn_3O_4 [154]. (E) HER polarisation curves of Pt/C, Ru/C, and Ru-ZrO_{2-x}/C catalysts. (F) Comparisons of the overpotentials at 10 mA cm^{-2}. (G) Mass activities of Ru/C, Pt/C, and Ru-ZrO_{2-x}/C catalysts and the hydrogen adsorption energies on the Ru(0001), Pt(111), and Ru-ZrO_{2-x} surfaces obtained from DFT calculations[155].

coupled electron transfer process of OER markedly diminishes the overall electrolysis rate[157-159]. Hence, there is a concerted effort among researchers to explore efficient OER catalysts. IrO_2/RuO_2 stands as a relatively advanced catalyst; however, its high cost is a barrier to further advancement[160,161]. Consequently, the quest for low-cost, high-efficiency, and stable OER catalysts has emerged as a focal point of research.

Zhu *et al.* have demonstrated the remarkable catalytic performance of plasma-treated TiO_2 nanowires (Ir@Sr-p-TiO_2 NWs) in the OER, achieving a substantial reduction in overpotential to 250 mV at a current density of 10 mA cm^{-2} [Figure 10A][162]. The inset in Figure 10A shows that the mass activity of Ir@Sr-p-TiO_2 NWs at a potential of 1.53 V is 1364.7 A g_{Ir}^{-1}, which is much higher than the mass activity of c-IrO_2 (24.9 A g_{Ir}^{-1}). This heightened activity is predominantly ascribed to the formation of O_v induced by plasma treatment and the adsorption of Sr on the p-TiO_2 nanomaterial, which reinforces the metal-support interaction between Ir nanoparticles and p-TiO_2 nanomaterials, which is beneficial to improve the stability of the catalyst. After 80 h of prolonged OER testing, these nanostructures maintained their activity without significant degradation and exhibited excellent stability compared to conventional c-IrO_2 catalysts [Figure 10B]. Wen *et al.* effectively synthesized spinel $Ni_xMn_{3-x}O_4$ solid solutions embedding single-atom iridium (Ir-SAs) via a sol-gel approach[163]. The presence of surface-exposed Ir-SAs in $Ir_1/Ni_{1.6}Mn_{1.4}O_4$ led to improved OER performance. Remarkable catalytic activity has been observed at high current densities, achieving overpotentials of 330 and 350 mV at current densities of 100 and 200 mA cm^{-2}, respectively [Figure 10C]. The research team further investigated the changes in charge distribution and the evolution pathway of OER in materials modified with single Ir atoms. Their preliminary investigation revealed alterations in the electronic structure of NiMnO upon Ir modification. Specifically, both d_{xy} and d_{xz} states of Ir atoms occupied half, indicating the high-spin state of Ir_1 in $Ni_{1.6}Mn_{1.4}O_4$, thereby enhancing the conductivity [Figure 10D].

ORR

The ORR occurring at the air cathode plays a critical role in energy conversion and storage technologies, such as rechargeable zinc-air batteries (ZABs). As a fundamental component of ZABs, the cathodic ORR

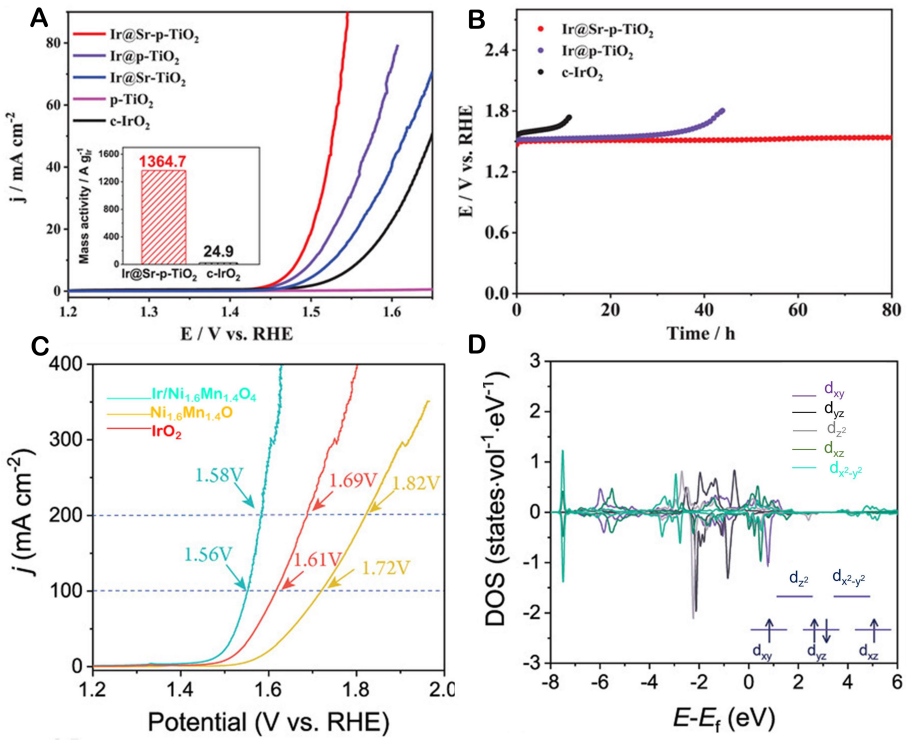

Figure 10. (A) OER polarization curves. The inset shows the mass activities of the catalysts. (B) Chronopotentiometric curves for OER[162]. (C) OER polarization curves with iR correction. (D) Calculated projected density of states of Ir atom[163].

exhibits slow reaction kinetics due to the high-energy barriers associated with O_2 adsorption, O-O bond cleavage, and the intricate reaction mechanisms involved[164-166]. Hence, the development of highly efficient catalysts is imperative. SACs have garnered extensive research interest owing to their ability to significantly enhance the number of active sites. Notably, their well-defined active centers elucidate the interactions between individual metal atoms and the supporting materials more clearly[167].

Zhang *et al.* proposed a ligand-assisted strategy to synthesize single-atom Fe-N-C derived from Zr-MOFs[168]. The resulting SA Fe@ZrO_2/nitrogen-doped carbon (NC) catalyst integrates FeN_4 sites and adjacent ZrO_2 into NC, with the *in-situ* introduced ZrO_2 significantly enhancing O_2 adsorption capacity. With a mesoporous structure, atomically dispersed Fe-N_4 active sites, and strong interface interactions between Fe atoms and ZrO_2 nanoclusters, the catalyst exhibited outstanding ORR activity in an alkaline solution, with an $E_{1/2}$ of 0.86 V, equivalent to Pt/C ($E_{1/2}$ = 0.86 V) [Figure 11A]. DFT calculations further elucidated that adjacent ZrO_2 nanoclusters effectively modulated the electronic structure of Fe atoms at FeN_4 sites, thereby enhancing the ORR process and activity. When conducting Bader charge analysis on SA Fe@ZrO_2/NC and SA Fe/NC [Figure 11B and C], the results indicate that oxygen molecules adsorbed on SA Fe@ZrO_2/NC acquire more charge compared to those adsorbed on SA Fe/NC. This suggests that the FeN_4 sites adjacent to ZrO_2 nanoclusters facilitate the reduction of oxygen molecules. Such findings elucidate the beneficial promotional effect of the presence of ZrO_2 nanoclusters on catalytic activity within this catalyst system. ul Haq *et al.* combined electrochemically etched $Nb_4C_3T_x$-MXene nanosheets with Fe-N-C SACs[169]. They introduced Fe-N-C SACs into oxygen-terminated $Nb_4C_3T_x$-MXene through a novel self-assembly technique. Fe-N-C/$Nb_4C_3T_x$ exhibited exceptional electrocatalytic performance for the ORR in alkaline conditions ($E_{1/2}$ = 0.911 V) [Figure 11D]. As shown in Figure 11E and F, the catalyst also possesses excellent stability. This remarkable activity stems from its large specific surface area, gradient porous

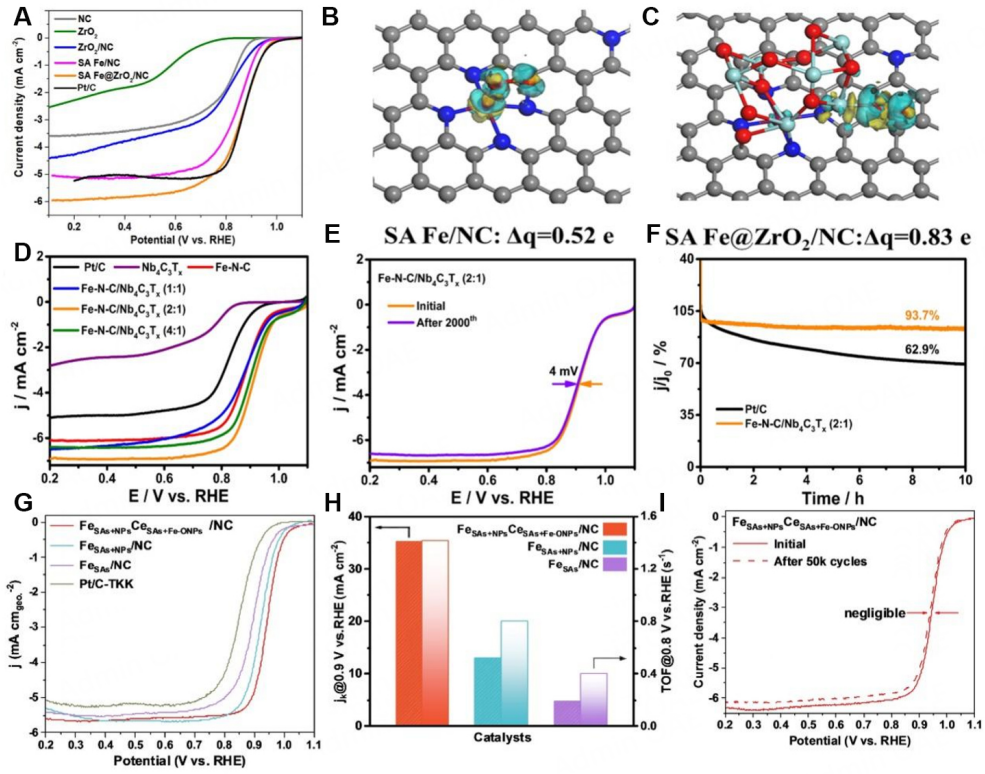

Figure 11. (A) LSV curves of Pt/C. (B and C) Differential charge density analysis of SA Fe/NC and SA Fe@ZrO_2/NC models. Light blue area represents charge density decrease, and yellow area denotes charge density increase[168]. (D) LSV curves of the catalysts for the ORR. (E) ORR curves of the Fe-N-C/$Nb_4C_3T_x$ (2:1) before and after sweeping for 2,000 cycles. (F) Chronoamperometric curves of the catalyst based on the Fe-N-C/$Nb_4C_3T_x$ (2:1)[169]. (G) ORR polarization curves. (H) j_k and TOF of catalysts to present intrinsic activity. (I) Durability results of the catalyst after 50,000 potential cycles[170].

structure, appropriate degree of graphitization, synergistic effects between components, and the presence of coordination-rich electron-donating metal ions. Xu *et al.* leveraging DFT in conjunction with machine learning (ML), conducted an in-depth exploration of the synergistic effects among FeN_4OH sites, CeN_4OH motifs, iron nanoparticles, and Fe-CeO_2 NPs[170]. This holistic effect entails a delicate interplay between electronic and geometric interactions, leading to a remarkable enhancement in the ORR activity of FeN_4OH active sites, with an $E_{1/2}$ reaching 0.948 V (V_{RHE}, voltage with respect to the reversible hydrogen electrode), surpassing the performance of commercial Pt/C ($E_{1/2}$ = 0.851 V_{RHE}) [Figure 11G]. $Fe_{SAs+NPs}Ce_{SAs+Fe-ONPs}$/NC exhibits exceptional durability, with negligible activity loss even after 50,000 cycles. This results from the excellent intrinsic activity and stability of the catalyst [Figure 11H and I]. The universality of this synergistic effect extends to multi-component systems based on Co, Ni, Cu, Cr, and Mn. These findings underscore the paramount importance of synergistic effects in simultaneously boosting catalytic activity and durability.

CO_2RR

To address the issue of global warming caused by CO_2 emissions from fossil fuel combustion, converting CO_2 into valuable chemical products such as carbon monoxide (CO), CH_4, and ethanol presents a promising strategy. The selection of catalysts plays a crucial role in the selectivity of the CO_2RR; thus, SACs with high catalytic activity have attracted significant attention.

Cao *et al.* have devised and screened 50 candidate SACs comprising $Ti_3C_2O_2$ coordinated with 25 TMs in N, S, or N, N configurations (NS/NN-$Ti_3C_2O_2$) for the CO_2RR to produce CO[171]. Through analysis of the limiting potential for CO production and competition with the formic acid generation, CO reduction, and HER, it was found that Ru-NS-$Ti_3C_2O_2$ and Co-NN-$Ti_3C_2O_2$ serve as outstanding catalysts for CO_2RR to generate CO. In actual electrocatalysis, Ru-NS-$Ti_3C_2O_2$ exhibited a remarkable electrochemical response; $E_b(CO_2)$ increases from 0.04 to 0.08 eV. The slight increase in $E_b(CO_2)$ is due to the negative CO_2 dipole, which leads to a slight inhibition of CO_2 adsorption at negative potential. When the electrode potential increases from 0 to -0.8 V, the reaction energy increases from 0.12 to 0.24 eV [Figure 12A], indicating significantly low reaction energies surpassing most reported catalysts to date. When we investigate the relation between binding energy and surface charge density, we can find that $E_b(CO_2)$, E_b(COOH), and E_b(CO) are linear with σ [Figure 12B]. This study introduces novel insights into the systematic and expeditious screening of candidate catalysts. Tan *et al.* proposed a novel strategy to stabilize copper using silicon dioxide and successfully synthesized $CuSiO_x$ amorphous nanotube catalysts featuring abundant atomic Cu-O-Si interfacial sites resistant to reconstruction[172]. The robust interfacial interaction between copper and silicon dioxide has endowed the Cu-O-Si interfacial sites with exceptional CO_2-to-CH_4 selectivity (72.5%) [Figure 12C]. When considering from the perspective of reaction thermodynamics, a higher value of $U_L(CO_2\text{-}*CO)\text{-}U_L(*H)$ corresponds to better selectivity towards CO_2 reduction. According to the data shown in Figure 12D, $CuSiO_x$ exhibits superior CO_2 reduction selectivity compared to metallic copper, effectively suppressing the competing HER. It becomes evident that the $\Delta G_{*COH}\text{-}\Delta G_{*OCCOH}$ value for $CuSiO_x$ is more negative compared to metallic copper. This observation suggests that protonation of *CO is more favorable at the Cu-O-Si atomic interface than on copper alone, thereby facilitating the generation process of CH_4. This research opens up a promising avenue for designing highly active and stable Cu-based CO_2 reduction catalysts. After conducting durability tests on the catalyst at a constant potential for 12 h, the activity of the catalyst remained basically consistent, mainly due to the SMSI between SiO_2 and Cu [Figure 12E].

NRR

Ammonia serves as the fundamental component for the production of the majority of fertilizers; thus, its production volume is crucial for today's food security[173]. However, the current production of NH_3 relies on fossil fuel consumption, prompting the search for sustainable production methods. Electrochemical NRR boasts higher energy efficiency and is poised to enable decentralized NH_3 production, ultimately potentially supporting distributed fertilizer manufacturing[174].

Zhang *et al.* have successfully synthesized lotus root-like amorphous TiO_2 nanofibers[175]. In contrast to previously reported Vacco-engineered TiO_2 nanocrystals, these fibers exhibit abundant intrinsic O_v and dangling bonds, resulting in significantly enhanced N_2 activation and electron transport capabilities. To address selectivity challenges, a confinement effect was achieved through V_o, leading to the successful synthesis of relatively isolated SAs and maximizing the availability of Ga-V_o reaction sites. DFT calculations indicated favorable N_2 adsorption on the catalyst surface by Ga SAs, while V_o facilitated N_2 activation and reduction. This synergistic activity/selectivity design resulted in high NH_3 yield (24.47 $g{\cdot}h^{-1}{\cdot}mg^{-1}$) and FE (48.64%) at remarkably low overpotentials [Figure 13A]. The catalyst was subjected to a long-term durability test for 24 h, and the time-series current measurement curve was stable, as shown in Figure 13B. Han *et al.* utilized a plasma-enhanced chemical vapor deposition technique in this investigation to immobilize TM elements onto two-dimensional conductive materials[176]. Among numerous trials, it was discovered that Ru SAs and Ru clusters supported on calcium titanate oxide demonstrated remarkable electrocatalytic capabilities (achieving NH_3 production rates of up to 137.5 ± 5.8 μg h^{-1} mg_{cat}^{-1}, as depicted in Figure 13C, surpassing the previous records for Ru-based catalysts. After five consecutive experiments, the

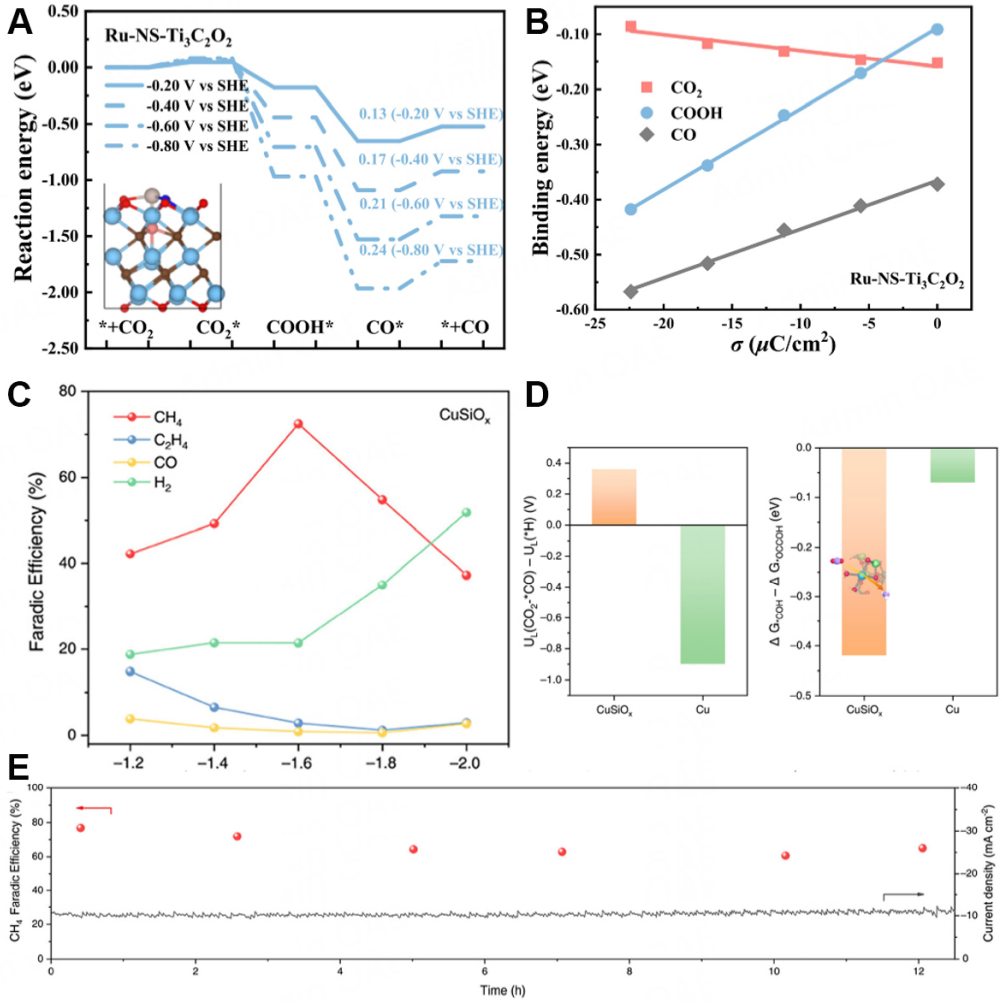

Figure 12. (A) Free energy diagram *vs.* SHE at different potentials on Ru-NS-$Ti_3C_2O_2$. (B) The binding energy of CO_2, COOH, and CO as a function of surface charge density (σ) for Ru-NS-$Ti_3C_2O_2$[171]. (C) FEs of CO_2RR products at different potentials. (D) Difference in limiting potentials for CO_2R and HER on $CuSiO_x$ and Cu (111), and reaction free energy difference between *CO protonation and C-C coupling steps on $CuSiO_x$ and Cu (111) surfaces. (E) $CuSiO_x$ reacts at a potential of -1.6 V *vs.* RHE for 12 h[172].

yield of LaFeO-Ru decreased by approximately 9%, from 137.3 μg h^{-1} $mgcat^{-1}$ to 124.7 μg h^{-1}, accompanied by a reduction in its efficiency of about 6.7%, dropping from 59.7% to 55.7% [Figure 13D]. These durability test results indicate a slight decline in the catalytic performance of LaFeO-Ru over prolonged usage, although it maintains relatively high catalytic activity and stability. This marginal performance degradation may be attributed to partial deactivation of the material surface or subtle structural alterations, warranting further investigation to comprehend its specific mechanisms.

Photocatalytic application

Single-atom photocatalysts have shown tremendous potential in the production of value-added chemicals and/or fuels, sparking considerable interest among researchers[177-179]. SAC photocatalysts refer to semiconductor substrates decorated with atomic-level metal particles. These metal atoms play the role of auxiliary catalysts on the semiconductor surface, increasing the number of active sites while receiving electrons from the process of light harvesting. Additionally, SAC photocatalysts can effectively reduce the usage of precious metals. This design offers higher catalytic efficiency and selectivity while lowering costs.

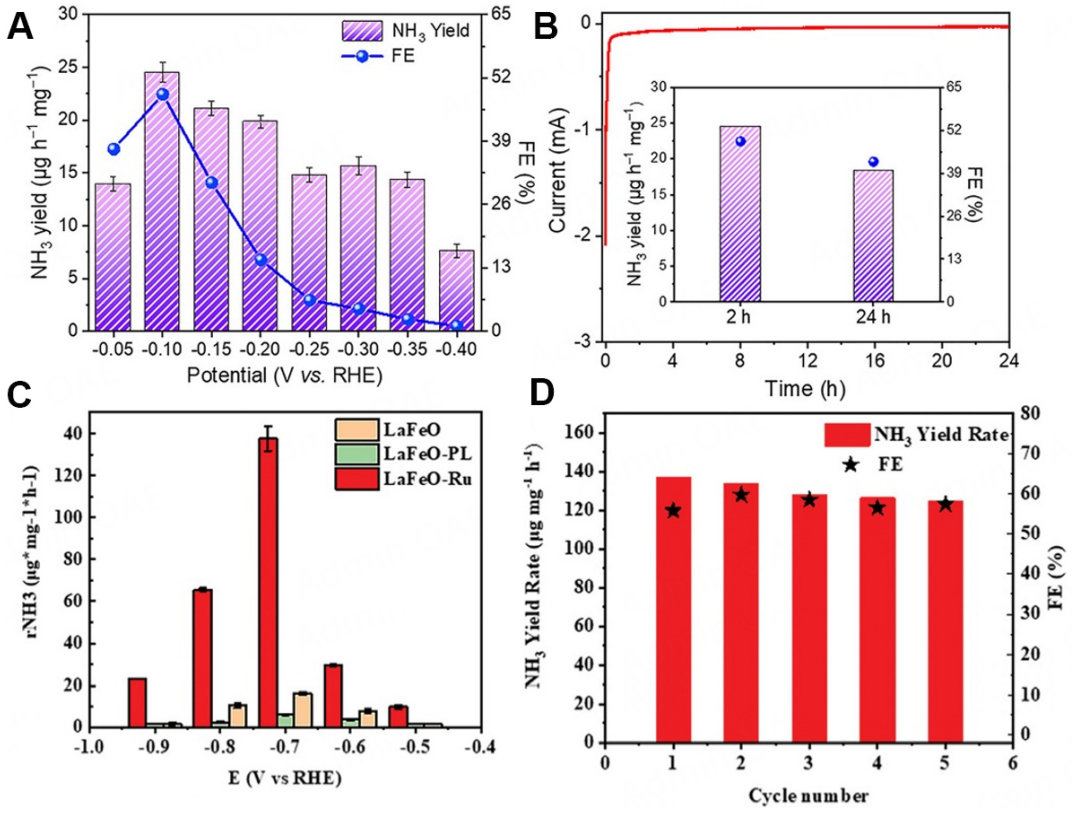

Figure 13. (A) NH_3 yields and FEs of Ga SA/a-TiO_2 nanofibers at different potentials for 2 h. (B) Chronoamperometry curve of Ga SA/a-TiO_2 nanofibers at -0.1 V *vs.* RHE for 24 h[175]. (C) NH_3 yield rates for LaFeO-Ru, LaFeO-PL, and LaFeO in the NRR. (D) FE and NH_3 yield rates for LaFeO-Ru at the potential of -0.7 V versus RHE after five consecutive experiments[176].

As a result, SAC photocatalysts have become one of the focal points of current research, with broad prospects for applications in fields such as energy conversion and environmental remediation[180-182]. In the field of photocatalysis research, photocatalytic hydrogen production is a focal point of investigation[183,184]. As one of the most promising photocatalysts, TiO_2 has the advantages of innocuity, abundant availability and good stability[185]. Kerketta *et al.* have confirmed that Grätzel-type mesoporous TiO_2 layers serve as ideal carriers for Pt SAs, facilitating efficient photocatalytic H_2 generation[186]. By optimizing the geometric structure and Pt SA loading layer, the research team achieved a high photocatalytic H_2 production rate of approximately 2,900 mL h^{-1} (under conditions of wavelength λ = 365 nm and light intensity I = 65 mW cm^{-2}) [Figure 14A]. The influence of TiO_2 layer thickness was also investigated. As can be seen from Figure 14B, the H_2 generation rate increases significantly with layer thickness, and reaches saturation at a thickness of 8 to 14 μm. This performance surpasses that of previous Pt_{SA}/TiO_2 structures based on TiO_2 nanotubes, nanosheets, or MOFs. Moreover, this SA/substrate combination exhibited highly stable H_2 production performance over some time. Lee *et al.* reported the design and synthesis of a highly active single-copper-atom Cu/TiO_2 photocatalyst, demonstrating reversible and synergistic photonic activation processes[187]. The research findings indicate that these reversible and synergistic activation processes occur at the single-atom level, enabling control over macroscopic photoelectric properties and subsequent enhancement of catalytic activity. Compared to pure TiO_2, Cu/TiO_2 exhibited a 34.0-fold increase in photocatalytic activity. The highest hydrogen production rate was achieved when the mass fraction of Cu/TiO_2 was 0.75 wt%, reaching 16.6 mmol g^{-1} h^{-1} [Figure 14C]; hydrogen generation remained stable over four consecutive cycles, with no noticeable decline in photocatalytic activity. During four consecutive experimental cycles, stable generation of H_2 was observed, as depicted in Figure 14D, where no significant decline in photocatalytic activity was

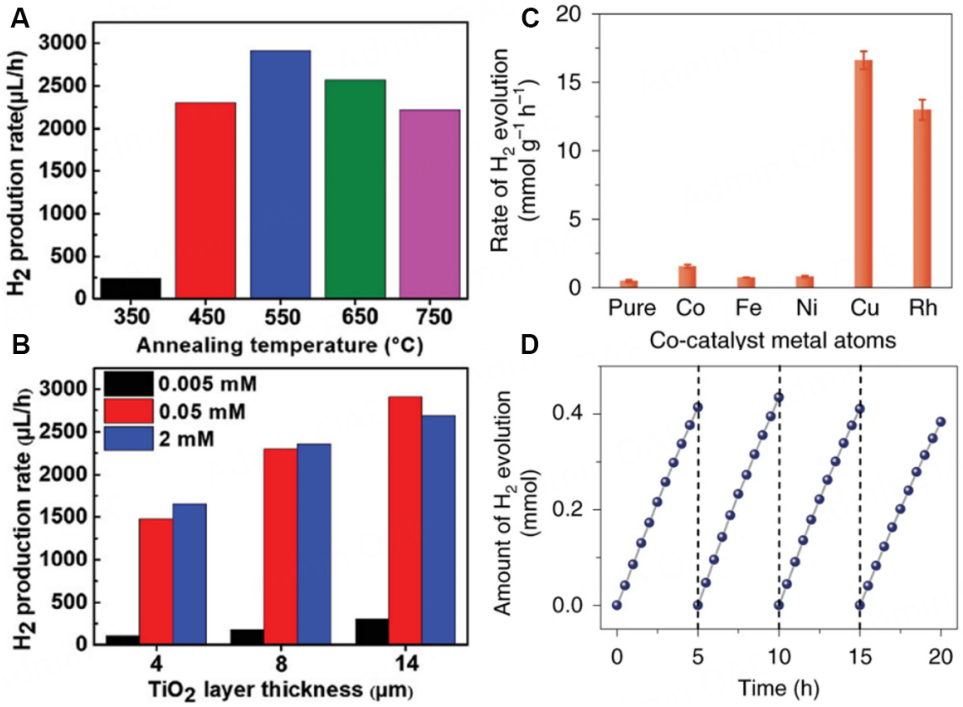

Figure 14. (A) The annealing temperature (using 14 μm layer thickness and 0.05 mM H_2PtCl_6 concentration in each case). (B) TiO_2 layer thickness and H_2PtCl_6 concentration (using annealing temperature of 550 °C in each case)[186]. (C) Rate of photocatalytic H_2 generation of M/TiO_2 (0.75 wt%) for each type of co-catalyst. (D) Cyclic measurements of photocatalytic H_2 generation of Cu/TiO_2 (0.75 wt%), showing the stable activity[187].

observed over this period. This outcome suggests that under the experimental conditions employed, the activity of the photocatalytic reaction remained stable throughout successive experimental cycles without any pronounced diminishing trend.

Converting carbon dioxide into valuable products via photocatalysis offers an eco-friendly solution to mitigate the greenhouse effect. Chen *et al.* reported an efficient photocatalytic system using two-dimensional $Ti_3C_2T_x$-MXene nanosheets as carriers, where individual cobalt atoms are anchored as active sites for CO_2 reduction under visible light[188]. In this system, $Ti_3C_2T_x$ nanosheets serve as bridges connecting the visible light absorber with cobalt active sites. Cobalt atoms form strong metal-oxygen/carbon bonds with $Ti_3C_2T_x$, resulting in the formation of the Co-$Ti_3C_2T_x$ integrated structure. The results show a CO production rate of up to 6.06 mmol h^{-1} g^{-1}, indicating significantly enhanced CO_2 photocatalytic performance compared to previous MXene-based catalysts. Theoretical calculations suggest that the synergistic interaction between isolated cobalt atoms and $Ti_3C_2T_x$ effectively promotes CO generation. Xu *et al.* have devised a novel heterogeneous photocatalyst by integrating Co-N-C with $BiFeO_3$ (BFO)[189]. Among these, the Co-N-C@BFO (1:7) catalyst demonstrated impressive yields in the reduction of CO_2 to CO and CH_4, reaching 1,373.41 and 169.32 μmol g^{-1}, respectively. In this study, the authors amalgamated displacement current, band theory, piezoelectric effect, and *in-situ* diffuse reflectance infrared Fourier transform spectroscopy to elucidate the mechanism. The amalgamation of the piezoelectric field and visible light facilitated charge separation, enhancing catalytic activity. In piezoelectric photocatalysis, the generation of displacement current resulted in a time-varying electrostatic potential, transferring electrons to the active sites of Co-N-C, thereby promoting CO_2RR. Additionally, the band alignment of BFO met the requisite criteria, further facilitating electron transfer to the active sites of Co-N-C for CO_2RR participation. The synergistic effect of the piezoelectric field and visible light promoted charge separation, thereby

augmenting catalytic activity. The introduction of noble metals into photocatalysts has been widely reported to effectively promote the activation of CO_2 molecules[190,191]. Li *et al.* successfully synthesized amorphous Al_2O_3 containing pentacoordinate aluminum (Al^V) using a solvothermal method and anchored gold (Au) SAs onto Al^V through a self-reduction strategy[192,193]. The introduction of the amorphous component weakened the Al-O bond energy, facilitating the release of oxygen atoms and leading to the transformation of the Al coordination environment to Al^V species[194]. Electron transfer between Al^V and Au stabilized the Au SAs. The introduction of Au SAs anchored on Al^V enhanced the chemical absorption capacity of CO_2, reduced the energy barrier for CO generation, and improved charge separation efficiency. Compared to pristine Al_2O_3, the CO generation rate significantly increased with Au SAs anchored, reaching approximately sixfold enhancement, with a CO selectivity of 98%. This work presents a straightforward synthetic method for Al^V species for the first time, elucidating the anchoring mechanism of Au SAs and providing important insights for the design of unsaturated coordination defects and anchoring SAs in photocatalysts.

Other catalytic applications

Presently, the conversion of carbon dioxide into liquid fuels stands as a viable strategy to combat contemporary energy and environmental issues. Recent years have witnessed significant advancements in carbon dioxide hydrogenation catalysts, particularly in the realm of SACs supported by oxides. Among these catalysts, the Fischer-Tropsch synthesis serves as a pivotal reaction process, directly impacting the coupling degree between carbon and the desired products[100,195].

Zhao *et al.* have presented an intriguing study unveiling a novel copper-based catalyst characterized by distinctive isolated active copper sites, exhibiting exceptional performance in CO hydrogenation[196]. With the CAZ^{-1} catalyst, only methanol was discerned, devoid of any accompanying byproducts. Notably, this catalyst showcased remarkable selectivity, prioritizing methanol production with an impressive TOF_{Cu} value reaching 1.37 h^{-1}. Their investigation reveals that the single-atom Cu-Zr catalyst predominantly facilitates methanol synthesis at 180 °C, whereas small copper clusters or nanoparticles with Cu-Cu structural motifs induce CO byproduct formation. Moreover, during the catalytic process, copper undergoes a transition from Cu-Cu structures to Cu_1-O_3 units, forming a catalyst surface with a quasi-planar structure, thereby expediting the hydrogenation of carbon dioxide. This seminal discovery not only underscores the pivotal roles of high activity, independent copper sites, and discernible structural motifs in the thermal catalytic hydrogenation of CO_2 but also presents novel conceptual frameworks for the application of SACs in energy conversion. Wu *et al.* synthesized adjustable ratio ZrO_2/Cu inverse catalysts using the oxalic acid co-precipitation method and discovered their remarkable performance in methanol production via CO_2 hydrogenation[197]. Under optimized conditions, the methanol mass yield of this catalyst reached 524 g_{MeOH} kg_{cat}^{-1} h^{-1}, surpassing that of traditional Cu/ZrO_2 catalysts by 3.3 times. Through in-depth investigation of its *in-situ* structure, they uncovered that the inverse ZrO_2/Cu catalyst adopted a unique island-like configuration with partially reduced amorphous ZrO_2 islands supported on Cu particles, where these ZrO_2 islands exhibited remarkable activity for CO_2 activation. Moreover, they observed the adsorption of formate intermediates on Cu, and under the inverse configuration, the activation of CO_2 and hydrogenation of surface oxygen intermediates were notably accelerated, providing insights into its exceptional methanol production activity. Zhou *et al.* observed significant differences when investigating Cu/Mo_2CT_x catalysts loaded on silicon dioxide compared to Cu/SiO_2 catalysts with similar copper loading[198]. Specifically, the intrinsic methanol production rate per unit mass of copper was significantly higher for Cu/Mo_2CT_x/SiO_2-2 h, with a rate over three times greater (1.51 *vs.* 0.41 gh^{-1} g_{Cu}^{-1}), while the methanol selectivity was slightly higher (54% compared to 45%). This finding is primarily attributed to the higher affinity of copper on partially reduced MXene surfaces and its greater mobility under high-temperature conditions. Furthermore, with prolonged reduction time, the Lewis acidity at the Cu/Mo_2CT_x

interface became stronger, further promoting the rate of CO_2 hydrogenation to methanol. This research highlights the potential advantages of Cu/Mo_2CT_x catalysts in CO_2 reduction reactions, providing valuable insights for the development of efficient CO_2 conversion catalysts.

CONCLUSIONS

This work provides a comprehensive review of the latest advancements in ceramic-supported SACs for catalysis. By thoroughly examining representative cases spanning oxides, perovskites, spinel, MXene, and other ceramic-based SACs, it reveals the intricate relationship between geometric and electronic structures of SACs and their corresponding performance. Oxides provide robust support for SACs due to their high thermal stability, chemical inertness, and high specific surface area, effectively stabilizing SA active centers. However, their poor conductivity and lack of redox activity limit their application. Spinel has various combinations and structures and excellent thermal stability, but its complex synthesis and high cost pose challenges to its widespread application. Perovskite exhibits structural flexibility, good oxygen migration, and conductivity. However, it is often prone to aggregation at high temperatures, and its high cost further limits its actual development. In contrast, MXene, as a novel 2D material, has high conductivity and abundant surface functional groups, although its complex synthesis process and long-term stability still require further investigation. Overall, ceramic supports play a crucial role in anchoring and isolating metal atoms while actively participating in catalytic reactions. By elucidating the complex interactions between metal atoms and ceramic carriers, insights are gained into the stability of atomic metal sites and the rational manipulation of individual atomic geometries and electronic structures. Additionally, this work systematically summarizes recent research progress in SACs, with a particular focus on advancements aimed at mitigating the migration or aggregation of isolated metal atoms. The review explores the applications of SACs in several pivotal catalytic reactions. Through detailed analysis of relevant theoretical research and reaction mechanisms, robust theoretical support is provided for the practical deployment of SACs in catalysis. Furthermore, this work highlights the advantages of SACs in the field of catalysis, including their exceptional catalytic performance, robust stability, and tunable electronic structure.

The research on SACs in the realm of catalysis continues to hold significant promise. As our understanding deepens, we anticipate the emergence of more innovative combinations of ceramic supports and metal atoms, thereby augmenting the catalytic performance and stability of SACs. The following points should be considered in future research.

(1) Research on the stability of metal atoms represents a critical avenue of investigation, with a central focus on preventing the migration or aggregation of isolated metal atoms. While several methods exist to achieve this objective, challenges persist. Consequently, future research will concentrate on developing more effective and stable anchoring strategies. These strategies will emphasize investigating the adsorption energy of metal atoms on various ceramic carriers, controlling the environment, and chemical states. Additionally, new synthesis strategies such as atomic layer deposition and self-assembly techniques will be developed to achieve uniform dispersion and stable anchoring of metal atoms. Through these efforts, we can gain a better understanding and control of the behavior of metal atoms in catalysis and other applications, laying the groundwork for designing more efficient materials and catalysts in the future.

(2) In-depth theoretical and experimental investigation of the catalytic mechanisms of SACs is crucial for driving advancements in this field. With the progress of computational simulation and theoretical studies, the development of ML-based catalyst design methods to predict optimal metal-carrier combinations has become a trend. By employing first-principles calculations to simulate the electronic structure, reaction intermediates, and energy conversion processes of SACs, and integrating experimental data such as X-ray

absorption spectroscopy and infrared spectroscopy, theoretical models and reaction pathways are validated. High-throughput computational screening is utilized to rapidly identify SACs with outstanding performance. It is anticipated that a substantial body of literature will emerge in the future, elucidating the catalytic mechanisms and reaction kinetics of SACs, and providing robust guidance for designing more efficient and stable SACs.

(3) One of the key tasks for future research is to develop low-cost, simple, and cost-effective methods for preparing SACs and exploring their broad applications in energy conversion, environmental protection, and other fields. Despite some reported methods for SACs preparation, they often suffer from issues such as high cost and complexity. Therefore, there is a need to seek simpler and more economically feasible preparation techniques to facilitate the practical application of SACs. This will help transition SACs from laboratory research to industrial applications and provide new solutions for addressing challenges in the fields of energy and environment.

(4) By innovatively designing ceramic supports, it is possible to achieve features with special electronic properties and surface activity, including aspects such as doping, heterostructures, and nanostructures. These designs are crucial in investigating the physicochemical properties of supports, as they directly influence the catalytic activity and selectivity of SACs. Further research will focus on exploring the performance optimization of SACs by adjusting the electronic structure and surface properties of the supports. Additionally, advanced preparation techniques such as sol-gel synthesis and deposition-precipitation methods can be considered to precisely control the morphology and structure of the supports. This aspect holds promise for providing new ideas and approaches for developing efficient and selective SACs, while also contributing to a deeper understanding of support-metal interactions, thereby laying the foundation for designing catalysts with enhanced activity and stability.

In conclusion, this work offers a comprehensive perspective and profound analysis of ceramic-based SACs in catalysis, delineating clear directions for future research. With the relentless progress of scientific inquiry and technological innovation, we believe SACs will increasingly shape the landscape of catalysis in the coming years.

DECLARATIONS

Authors' contributions

Made the literature review and drafted the original version: Jin C, Zhang Q
Revised the manuscript: Linda Akua Agyapomaa A, Zhang H, Zeng X
Conceived and supervised the project: Zeng X

Availability of data and materials

Not applicable.

Financial support and sponsorship

This work was supported by the National Natural Science Foundation of China (No. 22269010), the Jiangxi Provincial Natural Science Foundation (No. 20224BAB214021), and the Major Research Program of Jingdezhen Ceramic Industry (No. 2023ZDGG002).

Conflicts of interest

All authors declared that there are no conflicts of interest.

Ethical approval and consent to participate

Not applicable.

Consent for publication

Not applicable.

Copyright

REFERENCES

1. Zhang L, Zhao ZJ, Wang T, Gong J. Nano-designed semiconductors for electro- and photoelectro-catalytic conversion of carbon dioxide. *Chem Soc Rev* 2018;47:5423-43. DOI
2. Li D, Li X, Gong J. Catalytic reforming of oxygenates: state of the art and future prospects. *Chem Rev* 2016;116:11529-653. DOI
3. Subbaraman R, Tripkovic D, Chang KC, et al. Trends in activity for the water electrolyser reactions on 3D M(Ni,Co,Fe,Mn) hydr(oxy)oxide catalysts. *Nat Mater* 2012;11:550-7. DOI
4. Zhu J, Lv L, Zaman S, et al. Advances and challenges in single-site catalysts towards electrochemical CO_2 methanation. *Energy Environ Sci* 2023;16:4812-33. DOI
5. Tang C, Qiao SZ. How to explore ambient electrocatalytic nitrogen reduction reliably and insightfully. *Chem Soc Rev* 2019;48:3166-80. DOI PubMed
6. Zeng X, Shui J, Liu X, et al. Single-atom to single-atom grafting of Pt_1 onto Fe-N_4 center: Pt_1@Fe-N-C multifunctional electrocatalyst with significantly enhanced properties. *Adv Energy Mater* 2018;8:1701345. DOI
7. Liu J. Advanced electron microscopy of metal-support interactions in supported metal catalysts. *ChemCatChem* 2011;3:934-48. DOI
8. Schlögl R, Abd Hamid SB. Nanocatalysis: mature science revisited or something really new? *Angew Chem Int Ed* 2004;43:1628-37. DOI PubMed
9. Xia Y, Xiong Y, Lim B, Skrabalak SE. Shape-controlled synthesis of metal nanocrystals: simple chemistry meets complex physics? *Angew Chem Int Ed* 2009;48:60-103. DOI PubMed PMC
10. Bell AT. The impact of nanoscience on heterogeneous catalysis. *Science* 2003;299:1688-91. DOI PubMed
11. Li H, Li L, Li Y. The electronic structure and geometric structure of nanoclusters as catalytic active sites. *Nanotechnol Rev* 2013;2:515-28. DOI
12. Liu J, Gong H, Ye G, Fei H. Graphene oxide-derived single-atom catalysts for electrochemical energy conversion. *Rare Met* 2022;41:1703-26. DOI
13. Li R, Zhao J, Liu B, Wang D. Atomic distance engineering in metal catalysts to regulate catalytic performance. *Adv Mater* 2024;36:e2308653. DOI
14. McCardle K. Theoretical insights into single-atom catalysts. *Nat Comput Sci* 2022;2:138. DOI PubMed
15. Turner M, Golovko VB, Vaughan OPH, et al. Selective oxidation with dioxygen by gold nanoparticle catalysts derived from 55-atom clusters. *Nature* 2008;454:981-3. DOI
16. Vajda S, Pellin MJ, Greeley JP, et al. Subnanometre platinum clusters as highly active and selective catalysts for the oxidative dehydrogenation of propane. *Nat Mater* 2009;8:213-6. DOI
17. Lei Y, Mehmood F, Lee S, et al. Increased silver activity for direct propylene epoxidation via subnanometer size effects. *Science* 2010;328:224-8. DOI
18. Li J, Stephanopoulos MF, Xia Y. Introduction: heterogeneous single-atom catalysis. *Chem Rev* 2020;120:11699-702. DOI PubMed
19. Qiao B, Wang A, Yang X, et al. Single-atom catalysis of CO oxidation using Pt_1/FeO_x. *Nat Chem* 2011;3:634-41. DOI
20. Wang S, Min XT, Qiao B, Yan N, Zhang T. Single-atom catalysts: in search of the holy grails in catalysis. *Chin J Catal* 2023;52:1-13. DOI
21. Yang XF, Wang A, Qiao B, Li J, Liu J, Zhang T. Single-atom catalysts: a new frontier in heterogeneous catalysis. *ACC Chem Res* 2013;46:1740-8. DOI
22. Boronat M, Leyva-Pérez A, Corma A. Theoretical and experimental insights into the origin of the catalytic activity of subnanometric gold clusters: attempts to predict reactivity with clusters and nanoparticles of gold. *ACC Chem Res* 2014;47:834-44. DOI PubMed
23. Liu K, Zhao X, Ren G, et al. Strong metal-support interaction promoted scalable production of thermally stable single-atom catalysts. *Nat Commun* 2020;11:1263. DOI PubMed PMC
24. Wang A, Li J, Zhang T. Heterogeneous single-atom catalysis. *Nat Rev Chem* 2018;2:65-81. DOI
25. Lang R, Du X, Huang Y, et al. Single-atom catalysts based on the metal-oxide interaction. *Chem Rev* 2020;120:11986-2043. DOI
26. Xu Y, Zheng W, Liu X, et al. Platinum single atoms on tin oxide ultrathin films for extremely sensitive gas detection. *Mater Horiz* 2020;7:1519-27. DOI
27. Lan K, Wang R, Wei Q, et al. Stable Ti^{3+} defects in oriented mesoporous titania frameworks for efficient photocatalysis. *Angew Chem Int Ed* 2020;132:17829-36. DOI
28. Zheng T, Jiang K, Ta N, et al. Large-scale and highly selective CO_2 electrocatalytic reduction on nickel single-atom catalyst. *Joule*

2019;3:265-78. DOI

29. Kim MS, Lee J, Kim HS, et al. Heme cofactor-resembling Fe-N single site embedded graphene as nanozymes to selectively detect H_2O_2 with high sensitivity. *Adv Funct Mater* 2020;30:1905410. DOI
30. Liu L, Zhu QY, Li J, et al. Atomistic engineering of Ag/Pt nanoclusters for remarkably boosted mass electrocatalytic activity. *Energy Mater* 2022;2:200007. DOI
31. Ji S, Chen Y, Wang X, Zhang Z, Wang D, Li Y. Chemical synthesis of single atomic site catalysts. *Chem Rev* 2020;120:11900-55. DOI
32. Chen Y, Li H, Zhao W, et al. Optimizing reaction paths for methanol synthesis from CO_2 hydrogenation via metal-ligand cooperativity. *Nat Commun* 2019;10:1885. DOI PubMed PMC
33. Najam T, Ahmad Khan N, Ahmad Shah SS, et al. Metal-organic frameworks derived electrocatalysts for oxygen and carbon dioxide reduction reaction. *Chem Rec* 2022;22:e202100329. DOI
34. Guillon O. Ceramic materials for energy conversion and storage: a perspective. *Int J Ceram Eng Sci* 2021;3:100-4. DOI
35. Yang H, Wang CA, Dong Y. Energy ceramic design for robust battery cathodes and solid electrolytes. *Adv Powder Mater* 2024;3:100185. DOI
36. Wang F, Dong B, Wang J, et al. Self-supported porous heterostructure WC/WO_{3-x} ceramic electrode for hydrogen evolution reaction in acidic and alkaline media. *J Adv Ceram* 2022;11:1208-21. DOI
37. Yang J, Li W, Wang D, Li Y. Electronic metal-support interaction of single-atom catalysts and applications in electrocatalysis. *Adv Mater* 2020;32:e2003300. DOI
38. Zeng L, Xue C. Single metal atom decorated photocatalysts: progress and challenges. *Nano Res* 2021;14:934-44. DOI
39. Peng L, Shang L, Zhang T, Waterhouse GIN. Waterhouse GIN. Recent advances in the development of single-atom catalysts for oxygen electrocatalysis and zinc-air batteries. *Adv Energy Mater* 2020;10:2003018. DOI
40. Zhuang Z, Kang Q, Wang D, Li Y. Single-atom catalysis enables long-life, high-energy lithium-sulfur batteries. *Nano Res* 2020;13:1856-66. DOI
41. Hoang S, Guo Y, Binder AJ, et al. Activating low-temperature diesel oxidation by single-atom Pt on TiO_2 nanowire array. *Nat Commun* 2020;11:1062. DOI PubMed PMC
42. Kunwar D, Zhou S, Delariva A, et al. Stabilizing high metal loadings of thermally stable platinum single atoms on an industrial catalyst support. *ACS Catal* 2019;9:3978-90. DOI
43. Dvořák F, Farnesi Camellone M, Tovt A, et al. Creating single-atom Pt-ceria catalysts by surface step decoration. *Nat Commun* 2016;7:10801. DOI PubMed PMC
44. Qiao B, Liu J, Wang YG, et al. Highly efficient catalysis of preferential oxidation of CO in H_2-rich stream by gold single-atom catalysts. *ACS Catal* 2015;5:6249-54. DOI
45. Qiao B, Liang JX, Wang A, et al. Ultrastable single-atom gold catalysts with strong covalent metal-support interaction (CMSI). *Nano Res* 2015;8:2913-24. DOI
46. Liu J, Wang T, Liu X, et al. Reducible Co^{3+}-O sites of Co-Ni-P-O_x on CeO_2 nanorods boost acidic water oxidation via interfacial charge transfer-promoted surface reconstruction. *ACS Catal* 2023;13:5194-204. DOI
47. Yan S, Gao Z, Ding J, et al. Nanocomposites based on nanoceria regulate the immune microenvironment for the treatment of polycystic ovary syndrome. *J Nanobiotechnol* 2023;21:412. DOI PubMed PMC
48. Yavo N, Yeheskel O, Wachtel E, Ehre D, Frenkel AI, Lubomirsky I. Relaxation and saturation of electrostriction in 10 mol% Gd-doped ceria ceramics. *Acta Mater* 2018;144:411-8. DOI
49. Jones J, Xiong H, DeLaRiva AT, et al. Thermally stable single-atom platinum-on-ceria catalysts via atom trapping. *Science* 2016;353:150-4. DOI
50. Nie L, Mei D, Xiong H, et al. Activation of surface lattice oxygen in single-atom Pt/CeO_2 for low-temperature CO oxidation. *Science* 2017;358:1419-23. DOI
51. Beniya A, Higashi S. Towards dense single-atom catalysts for future automotive applications. *Nat Catal* 2019;2:590-602. DOI
52. Farmer JA, Campbell CT. Ceria maintains smaller metal catalyst particles by strong metal-support bonding. *Science* 2010;329:933-6. DOI PubMed
53. Corma A, Atienzar P, García H, Chane-Ching JY. Hierarchically mesostructured doped CeO_2 with potential for solar-cell use. *Nat Mater* 2004;3:394-7. DOI PubMed
54. Prieur D, Bonani W, Popa K, et al. Size dependence of lattice parameter and electronic structure in CeO_2 nanoparticles. *Inorg Chem* 2020;59:5760-7. DOI
55. Paun C, Safonova OV, Szlachetko J, et al. Polyhedral CeO_2 nanoparticles: size-dependent geometrical and electronic structure. *J Phys Chem C* 2012;116:7312-7. DOI
56. Xu J, Harmer J, Li G, et al. Size dependent oxygen buffering capacity of ceria nanocrystals. *Chem Commun* 2010;46:1887-9. DOI
57. Wang Y, Chen Z, Han P, et al. Single-atomic Cu with multiple oxygen vacancies on ceria for electrocatalytic CO_2 reduction to CH_4. *ACS Catal* 2018;8:7113-9. DOI
58. Xu J, Wang Y, Wang K, et al. Single-atom Rh on high-index CeO_2 facet for highly enhanced catalytic CO oxidation. *Angew Chem Int Ed* 2023;62:e202302877. DOI
59. Ruan X, Li S, Huang C, Zheng W, Cui X, Ravi SK. Catalyzing artificial photosynthesis with TiO_2 heterostructures and hybrids: emerging trends in a classical yet contemporary photocatalyst. *Adv Mater* 2024;36:e2305285. DOI

60. Martinez-Oviedo A, Kshetri YK, Joshi B, Lee SW. Surface modification of blue TiO_2 with silane coupling agent for NOx abatement. *Prog Nat Sci* 2021;31:230-8. DOI
61. Kuai L, Chen Z, Liu S, et al. Titania supported synergistic palladium single atoms and nanoparticles for room temperature ketone and aldehydes hydrogenation. *Nat Commun* 2020;11:48. DOI PubMed PMC
62. Han B, Guo Y, Huang Y, et al. Strong metal-support interactions between Pt single atoms and TiO_2. *Angew Chem Int Ed* 2020;59:11824-9. DOI
63. Chen Y, Ji S, Sun W, et al. Engineering the atomic interface with single platinum atoms for enhanced photocatalytic hydrogen production. *Angew Chem Int Ed* 2020;132:1311-7. DOI
64. Wan J, Chen W, Jia C, et al. Defect effects on TiO_2 nanosheets: stabilizing single atomic site Au and promoting catalytic properties. *Adv Mater* 2018:30. DOI
65. Yang M, Allard LF, Flytzani-Stephanopoulos M. Atomically dispersed Au-$(OH)_x$ species bound on titania catalyze the low-temperature water-gas shift reaction. *J Am Chem Soc* 2013;135:3768-71. DOI PubMed
66. Xu H, Liu C, Guo W, et al. Sodium alginate/Al_2O_3 fiber nanocomposite aerogel with thermal insulation and flame retardancy properties. *Chem Eng J* 2024;489:151223. DOI
67. Hu J, Gao T, Li M, Liu X. Synthesis of an (Al_3BC + Al_2O_3)/Al composite with high stiffness and attractive high-temperature tensile properties. *Mater Res Lett* 2024;12:355-62. DOI
68. Zhao L, Liang Y, Ma J, et al. Ultra-steep-slope and high-stability of $CuInP_2S_6$/WS_2 ferroelectric negative capacitor transistors by passivation effect and dual-gate modulation. *Adv Funct Mater* 2023;33:2306708. DOI
69. Li H, Hu J, Zhang Y, et al. Single-transistor optoelectronic spiking neuron with optogenetics-inspired spatiotemporal dynamics. *Adv Funct Mater* 2024;34:2314456. DOI
70. Wang F, Ma J, Xin S, et al. Resolving the puzzle of single-atom silver dispersion on nanosized γ-Al_2O_3 surface for high catalytic performance. *Nat Commun* 2020;11:529. DOI PubMed PMC
71. Qin R, Zhou L, Liu P, et al. Alkali ions secure hydrides for catalytic hydrogenation. *Nat Catal* 2020;3:703-9. DOI
72. Yang K, Liu Y, Deng J, et al. Three-dimensionally ordered mesoporous iron oxide-supported single-atom platinum: highly active catalysts for benzene combustion. *Appl Catal B Environ Energy* 2019;244:650-9. DOI
73. Parastaev A, Muravev V, Huertas Osta E, et al. Boosting CO_2 hydrogenation via size-dependent metal-support interactions in cobalt/ceria-based catalysts. *Nat Catal* 2020;3:526-33. DOI
74. van Deelen TW, Hernández Mejía C, de Jong KP. Control of metal-support interactions in heterogeneous catalysts to enhance activity and selectivity. *Nat Catal* 2019;2:955-70. DOI
75. Liu SR, Luo ST, Wu XD, et al. Application of silica-alumina as hydrothermally stable supports for Pt catalysts for acid-assisted soot oxidation. *Rare Met* 2023;42:1614-23. DOI
76. Vaudry F, Khodabandeh S, Davis ME. Synthesis of pure alumina mesoporous materials. *Chem Mater* 1996;8:1451-64. DOI
77. Li W, Kovarik L, Mei D, et al. A general mechanism for stabilizing the small sizes of precious metal nanoparticles on oxide supports. *Chem Mater* 2014;26:5475-81. DOI
78. Shang H, Chen W, Jiang Z, Zhou D, Zhang J. Atomic-dispersed platinum anchored on porous alumina sheets as an efficient catalyst for diboration of alkynes. *Chem Commun* 2020;56:3127-30. DOI
79. Zhang Z, Zhu Y, Asakura H, et al. Thermally stable single atom Pt/m-Al_2O_3 for selective hydrogenation and CO oxidation. *Nat Commun* 2017;8:16100. DOI PubMed PMC
80. Lan F, Zhang H, Zhao C, Shu Y, Guan Q, Li W. Copper clusters encapsulated in carbonaceous mesoporous silica nanospheres for the valorization of biomass-derived molecules. *ACS Catal* 2022;12:5711-25. DOI
81. Zhang D, Cai H, Su Y, Sun W, Yang D, Ozin GA. Silica samurai: aristocrat of energy and environmental catalysis. *Chem Catal* 2022;2:1893-918. DOI
82. Pellico J, Vass L, Carrascal-Miniño A, et al. In vivo real-time positron emission particle tracking (PEPT) and single particle PET. *Nat Nanotechnol* 2024;19:668-76. DOI PubMed PMC
83. Du J, Liu B, Zhao T, et al. Silica nanoparticles protect rice against biotic and abiotic stresses. *J Nanobiotechnol* 2022;20:197. DOI PubMed PMC
84. Rice SB, Koo JY, Disko MM, Treacy MMJ. On the imaging of Pt atoms in zeolite frameworks. *Ultramicroscopy* 1990;34:108-18. DOI
85. Maschmeyer T, Rey F, Sankar G, Thomas JM. Heterogeneous catalysts obtained by grafting metallocene complexes onto mesoporous silica. *Nature* 1995;378:159-62. DOI
86. Duan H, Li M, Zhang G, et al. Single-site palladium (II) catalyst for oxidative heck reaction: catalytic performance and kinetic investigations. *ACS Catal* 2015;5:3752-9. DOI
87. Wu W, Cui E, Zhang Y, et al. Involving single-atom silver(0) in selective dehalogenation by AgF under visible-light irradiation. *ACS Catal* 2019;9:6335-41. DOI
88. Zhang H, Zeng X, Zhang Q, Zhang Z, Jin C, Yu R. Dual template-induced construction of three-dimensional porous SiO_2/NC/Co-CNTs heterostructure with highly dispersed active sites for efficient oxygen evolution reaction. *Tungsten* 2024;6:585-95. DOI
89. Yang M, Li S, Wang Y, et al. Catalytically active Au-O$(OH)_x$-species stabilized by alkali ions on zeolites and mesoporous oxides. *Science* 2014;346:1498-501. DOI
90. De S, Babak MV, Hülsey MJ, Ang WH, Yan N. Designed precursor for the controlled synthesis of highly active atomic and sub-

nanometric platinum catalysts on mesoporous silica. *Chem Asian J* 2018;13:1053-9. DOI PubMed

91. Zhai Y, Pierre D, Si R, et al. Alkali-stabilized Pt-OH_x species catalyze low-temperature water-gas shift reactions. *Science* 2010;329:1633-6. DOI
92. Sun Q, Wang N, Xu Q, Yu J. Nanopore-supported metal nanocatalysts for efficient hydrogen generation from liquid-phase chemical hydrogen storage materials. *Adv Mater* 2020;32:e2001818. DOI PubMed
93. Li X, Pereira-Hernández XI, Chen Y, et al. Functional CeO_x nanoglues for robust atomically dispersed catalysts. *Nature* 2022;611:284-8. DOI
94. Mokhtar M, Basahel SN, Ali TT. Effect of synthesis methods for mesoporous zirconia on its structural and textural properties. *J Mater Sci* 2013;48:2705-13. DOI
95. Jia K, Zheng L, Liu W, et al. A new and simple way to prepare monolithic solid oxide fuel cell stack by stereolithography 3D printing technology using 8 mol% yttria stabilized zirconia photocurable slurry. *J Eur Ceram Soc* 2022;42:4275-85. DOI
96. Chang CH, Lin CY, Chang CH, Liu FH, Huang YT, Liao YS. Enhanced biomedical applicability of ZrO_2-SiO_2 ceramic composites in 3D printed bone scaffolds. *Sci Rep* 2022;12:6845. DOI PubMed PMC
97. Wang S, Li X, Wang J, et al. Enhanced electromechanical properties in $MnCO_3$-modified Pb(Ni, Nb)O_3-$PbZrO_3$-$PbTiO_3$ ceramics via defect and domain engineering. *J Am Ceram Soc* 2023;106:1970-80. DOI
98. Pokrovski K, Jung KT, Bell AT. Investigation of CO and CO_2 adsorption on tetragonal and monoclinic zirconia. *Langmuir* 2001;17:4297-303. DOI
99. Wang J, Li G, Li Z, et al. A highly selective and stable ZnO-ZrO_2 solid solution catalyst for CO_2 hydrogenation to methanol. *Sci Adv* 2017;3:e1701290. DOI PubMed PMC
100. Wang Y, Kattel S, Gao W, et al. Exploring the ternary interactions in Cu-ZnO-ZrO_2 catalysts for efficient CO_2 hydrogenation to methanol. *Nat Commun* 2019;10:1166. DOI PubMed PMC
101. Samson K, Śliwa M, Socha RP, et al. Influence of ZrO_2 structure and copper electronic state on activity of Cu/ZrO_2 catalysts in methanol synthesis from CO_2. *ACS Catal* 2014;4:3730-41. DOI
102. Arena F, Barbera K, Italiano G, Bonura G, Spadaro L, Frusteri F. Synthesis, characterization and activity pattern of Cu-ZnO/ZrO_2 catalysts in the hydrogenation of carbon dioxide to methanol. *J Catal* 2007;249:185-94. DOI
103. Guo X, Mao D, Lu G, Wang S, Wu G. Glycine-nitrate combustion synthesis of CuO-ZnO-ZrO_2 catalysts for methanol synthesis from CO_2 hydrogenation. *J Catal* 2010;271:178-85. DOI
104. Kondratenko EV, Mul G, Baltrusaitis J, Larrazábal GO, Pérez-ramírez J. Status and perspectives of CO_2 conversion into fuels and chemicals by catalytic, photocatalytic and electrocatalytic processes. *Energy Environ Sci* 2013;6:3112. DOI
105. Du W, Sun Z, Chen K, Wang F, Chu K. Nb1-Zr dual active sites constructed on ZrO_2 boost nitrite-to-ammonia electroreduction. *Chem Eng J* 2024;481:148733. DOI
106. Choudhary N, Jiang S, Pham H, et al. Precisely designed cobalt single atom on ZrO_2 support for chemical CO_2 fixation. *Appl Catal B Environ Energy* 2024;344:123627. DOI
107. Huang J, Han J, Wang R, et al. Improving electrocatalysts for oxygen evolution using $Ni_xFe_{3-x}O_4$/Ni hybrid nanostructures formed by solvothermal synthesis. *ACS Energy Lett* 2018;3:1698-707. DOI
108. Thackeray MM, Amine K. $Li_4Ti_5O_{12}$ spinel anodes *Nat Energy* 2021;6:683. DOI
109. Liu X, He L, Han G, Sheng J, Yu Y, Yang W. Design of rich defects carbon coated $MnFe_2O_4$/$LaMnO_3$/$LaFeO_3$ heterostructure nanocomposites for broadband electromagnetic wave absorption. *Chem Eng J* 2023;476:146199. DOI
110. Liu X, Duan Y, Guo Y, et al. In situ construction of complex spinel ferrimagnet in multi-elemental alloy for modulating natural resonance and highly efficient electromagnetic absorption. *Chem Eng J* 2023;462:142200. DOI
111. Avcı ÖN, Sementa L, Fortunelli A. Mechanisms of the oxygen evolution reaction on $NiFe_2O_4$ and $CoFe_2O_4$ inverse-spinel oxides. *ACS Catal* 2022;12:9058-73. DOI PubMed PMC
112. Rushiti A, Hättig C, Wen B, Selloni A. Structure and reactivity of pristine and reduced spinel $CoFe_2O_4$ (001)/(100) surfaces. *J Phys Chem C* 2021;125:9774-81. DOI
113. Zhu H, Zhang S, Huang YX, Wu L, Sun S. Monodisperse $M_xFe_{3-x}O_4$ (M= Fe, Cu, Co, Mn) nanoparticles and their electrocatalysis for oxygen reduction reaction. *Nano Lett* 2013;13:2947-51. DOI
114. Liu J, Zhu D, Ling T, Vasileff A, Qiao S. S-$NiFe_2O_4$ ultra-small nanoparticle built nanosheets for efficient water splitting in alkaline and neutral pH. *Nano Energy* 2017;40:264-73. DOI
115. Sun S, Sun Y, Zhou Y, et al. Shifting oxygen charge towards octahedral metal: a way to promote water oxidation on cobalt spinel oxides. *Angew Chem Int Ed* 2019;131:6103-8. DOI
116. Zhou Y, Sun S, Wei C, et al. Significance of engineering the octahedral units to promote the oxygen evolution reaction of spinel oxides. *Adv Mater* 2019;31:e1902509. DOI
117. Geng KQ, Yang MQ, Meng JX, et al. Engineering layered/spinel heterostructure via molybdenum doping towards highly stable Li-rich cathodes. *Tungsten* 2022;4:323-35. DOI
118. Shan J, Ye C, Chen S, et al. Short-range ordered iridium single atoms integrated into cobalt oxide spinel structure for highly efficient electrocatalytic water oxidation. *J Am Chem Soc* 2021;143:5201-11. DOI
119. Wang Y, Zhu YQ, Xie Z, et al. Efficient electrocatalytic oxidation of glycerol via promoted OH* generation over single-atom-bismuth-doped spinel Co_3O_4. *ACS Catal* 2022;12:12432-43. DOI
120. Yin WJ, Weng B, Ge J, Sun Q, Li Z, Yan Y. Oxide perovskites, double perovskites and derivatives for electrocatalysis,

photocatalysis, and photovoltaics. *Energy Environ Sci* 2019;12:442-62. DOI

121. Sun C, Alonso JA, Bian J. Recent advances in perovskite-type oxides for energy conversion and storage applications. *Adv Energy Mater* 2021;11:2000459. DOI
122. Song HJ, Yoon H, Ju B, Kim D. Highly efficient perovskite-based electrocatalysts for water oxidation in acidic environments: a mini review. *Adv Energy Mater* 2021;11:2002428. DOI
123. Sutherland LJ, Benitez-rodriguez J, Vak D, et al. A high-pressure isostatic lamination technique to fabricate versatile carbon electrode-based perovskite solar cells. *Commun Mater* 2024;5:90. DOI
124. Hailegnaw B, Demchyshyn S, Putz C, et al. Flexible quasi-2D perovskite solar cells with high specific power and improved stability for energy-autonomous drones. *Nat Energy* 2024;9:677-90. DOI
125. Xia Y, Zhu M, Qin L, et al. Organic-inorganic hybrid quasi-2D perovskites incorporated with fluorinated additives for efficient and stable four-terminal tandem solar cells. *Energy Mater* 2023;3:300004. DOI
126. Zhang D, Wang Y, Peng Y, et al. Novel high-entropy perovskite-type symmetrical electrode for efficient and durable carbon dioxide reduction reaction. *Adv Powder Mater* 2023;2:100129. DOI
127. Dai J, Zhu Y, Tahini HA, et al. Single-phase perovskite oxide with super-exchange induced atomic-scale synergistic active centers enables ultrafast hydrogen evolution. *Nat Commun* 2020;11:5657. DOI PubMed PMC
128. Jung JI, Jeong HY, Kim MG, Nam G, Park J, Cho J. Fabrication of $Ba_{0.5}Sr_{0.5}Co_{0.8}Fe_{0.2}O_{(3-\delta)}$ catalysts with enhanced electrochemical performance by removing an inherent heterogeneous surface film layer. *Adv Mater* 2015;27:266-71. DOI PubMed
129. Nishihata Y, Mizuki J, Akao T, et al. Self-regeneration of a Pd-perovskite catalyst for automotive emissions control. *Nature* 2002;418:164-7. DOI
130. Tanaka H, Taniguchi M, Uenishi M, et al. Self-regenerating Rh- and Pt-based perovskite catalysts for automotive-emissions control. *Angew Chem Int Ed* 2006;45:5998-6002. DOI
131. Onn TM, Monai M, Dai S, et al. Smart Pd catalyst with improved thermal stability supported on high-surface-area $LaFeO_3$ prepared by atomic layer deposition. *J Am Chem Soc* 2018;140:4841-8. DOI
132. Tian C, Zhang H, Zhu X, et al. A new trick for an old support: Stabilizing gold single atoms on $LaFeO_3$ perovskite. *Appl Catal B Environ Energy* 2020;261:118178. DOI
133. Shin H, Ko J, Park C, et al. Sacrificial template-assisted synthesis of inorganic nanosheets with high-loading single-atom catalysts: a general approach. *Adv Funct Mater* 2022;32:2110485. DOI
134. Niu S, Yang J, Qi H, et al. Single-atom Pt promoted Mo_2C for electrochemical hydrogen evolution reaction. *J Energy Chem* 2021;57:371-7. DOI
135. Zeng X, Ye Y, Wang Y, Yu R, Moskovits M, Stucky GD. Honeycomb-like MXene/$NiFeP_x$-NC with "continuous" single-crystal enabling high activity and robust durability in electrocatalytic oxygen evolution reactions. *J Adv Ceram* 2023;12:553-64. DOI
136. Zhang Z, Liang T, Jin C, et al. Synergistically coupling CoS/FeS_2 heterojunction nanosheets on a MXene *via* a dual molten salt etching strategy for efficient oxygen evolution reaction. *J Mater Chem A* 2024;12:14517-30. DOI
137. Zeng X, Jiang X, Ning Y, Gao Y, Che R. Constructing built-in electric fields with semiconductor junctions and Schottky junctions based on Mo-MXene/Mo-metal sulfides for electromagnetic response. *Nanomicro Lett* 2024;16:213. DOI PubMed PMC
138. Jin C, Peng H, Zeng X, Liu Z, Ding D. Hierarchical assembly of NiFe-PB-derived bimetallic phosphides on 3D Ti_3C_2 MXene ribbon networks for efficient oxygen evolution. *ChemPhysMater* 2024;3:118-24. DOI
139. Yu LH, Tao X, Feng SR, et al. Recent development of three-dimension printed graphene oxide and MXene-based energy storage devices. *Tungsten* 2024;6:196-211. DOI
140. Zeng X, Tan Y, Xia L, Zhang Q, Stucky GD. MXene-derived Ti_3C_2-Co-TiO_2 nanoparticle arrays via cation exchange for highly efficient and stable electrocatalytic oxygen evolution. *Chem Commun* 2023;59:880-3. DOI
141. Luo J, Gao S, Luo H, et al. Superhydrophobic and breathable smart MXene-based textile for multifunctional wearable sensing electronics. *Chem Eng J* 2021;406:126898. DOI
142. Wu X, Han B, Zhang H, et al. Compressible, durable and conductive polydimethylsiloxane-coated MXene foams for high-performance electromagnetic interference shielding. *Chem Eng J* 2020;381:122622. DOI
143. Zhong Q, Li Y, Zhang G. Two-dimensional MXene-based and MXene-derived photocatalysts: recent developments and perspectives. *Chem Eng J* 2021;409:128099. DOI
144. Zeng X, Duan D, Zhang X, et al. Doping and interface engineering in a sandwich $Ti_3C_2T_x$/$MoS_{2-x}P_x$ heterostructure for efficient hydrogen evolution. *J Mater Chem C* 2022;10:4140-7. DOI
145. Zeng X, Zhao C, Jiang X, Yu R, Che R. Functional tailoring of multi-dimensional pure MXene nanostructures for significantly accelerated electromagnetic wave absorption. *Small* 2023;19:e2303393. DOI
146. Zeng X, Jiang X, Ning Y, Hu F, Fan B. Construction of dual heterogeneous interface between zigzag-like Mo-MXene nanofibers and small CoNi@NC nanoparticles for electromagnetic wave absorption. *J Adv Ceram* 2023;12:1562-76. DOI
147. Ramalingam V, Varadhan P, Fu HC, et al. Heteroatom-mediated interactions between ruthenium single atoms and an MXene support for efficient hydrogen evolution. *Adv Mater* 2019;31:e1903841. DOI
148. Zhang J, Wang E, Cui S, Yang S, Zou X, Gong Y. Single-atom Pt anchored on oxygen vacancy of monolayer $Ti_3C_2T_x$ for superior hydrogen evolution. *Nano Lett* 2022;22:1398-405. DOI
149. Zeng X, Zhang H, Yu R, Stucky GD, Qiu J. A phase and interface co-engineered MoP_xS_y@$NiFeP_xS_y$@NPS-C hierarchical heterostructure for sustainable oxygen evolution reaction. *J Mater Chem A* 2023;11:14272-83. DOI

150. Luo F, Yu Y, Long X, Li C, Xiong T, Yang Z. Boosting catalytic activity toward methanol oxidation reaction for platinum via heterostructure engineering. *J Colloid Interface Sci* 2024;656:450-6. DOI
151. Seh ZW, Kibsgaard J, Dickens CF, Chorkendorff I, Nørskov JK, Jaramillo TF. Combining theory and experiment in electrocatalysis: insights into materials design. *Science* 2017;355:eaad4998. DOI PubMed
152. Zeng X, Zhang Q, Shen Z, Zhang H, Wang T, Liu Z. Doping and vacancy engineering in a sandwich-like g-C_3N_4/$NiCo_2O_4$ heterostructure for robust oxygen evolution. *ChemNanoMat* 2022;8:e202200191. DOI
153. Jing H, Zhu P, Zheng X, Zhang Z, Wang D, Li Y. Theory-oriented screening and discovery of advanced energy transformation materials in electrocatalysis. *Adv Powder Mater* 2022;1:100013. DOI
154. Wei J, Xiao K, Chen Y, Guo X, Huang B, Liu Z. *In situ* precise anchoring of Pt single atoms in spinel Mn_3O_4 for a highly efficient hydrogen evolution reaction. *Energy Environ Sci* 2022;15:4592-600. DOI
155. Kim M, Kim S, Park J, et al. Reconstructing oxygen-deficient zirconia with ruthenium catalyst on atomic-scale interfaces toward hydrogen production. *Adv Funct Mater* 2023;33:2300673. DOI
156. Navarra MA, Croce F, Scrosati B. New, high temperature superacid zirconia-doped Nafion™ composite membranes. *J Mater Chem* 2007;17:3210. DOI
157. Fabbri E, Habereder A, Waltar K, Kötz R, Schmidt TJ. Developments and perspectives of oxide-based catalysts for the oxygen evolution reaction. *Catal Sci Technol* 2014;4:3800-21. DOI
158. Zeng X, Zhang Q, Jin C, Huang H, Gao Y. Fe-induced electronic transfer and structural evolution of lotus pod-like $CoNiFeP_x$@P, N-C heterostructure for sustainable oxygen evolution. *Energy Environ Mater* 2024;7:e12628. DOI
159. Long X, Xiong T, Bao H, et al. Tip and heterogeneous effects co-contribute to a boosted performance and stability in zinc air battery. *J Colloid Interface Sci* 2024;662:676-85. DOI
160. Nguyen DC, Luyen Doan TL, Prabhakaran S, et al. Hierarchical Co and Nb dual-doped MoS_2 nanosheets shelled micro-TiO_2 hollow spheres as effective multifunctional electrocatalysts for HER, OER, and ORR. *Nano Energy* 2021;82:105750. DOI
161. Liu J, Liu X, Shi H, et al. Breaking the scaling relations of oxygen evolution reaction on amorphous NiFeP nanostructures with enhanced activity for overall seawater splitting. *Appl Catal B Environ Energy* 2022;302:120862. DOI
162. Zhu H, Wang Y, Jiang Z, Deng B, Xin Y, Jiang Z. Defect engineering promoted ultrafine Ir nanoparticle growth and Sr single-atom adsorption on TiO_2 nanowires to achieve high-performance overall water splitting in acidic media. *Adv Energy Mater* 2024;14:2303987. DOI
163. Wen N, Xia Y, Wang H, et al. Large-scale synthesis of spinel $Ni_xMn_{3-x}O_4$ solid solution immobilized with iridium single atoms for efficient alkaline seawater electrolysis. *Adv Sci* 2022;9:e2200529. DOI PubMed PMC
164. Pan J, Xu YY, Yang H, Dong Z, Liu H, Xia BY. Advanced architectures and relatives of air electrodes in Zn-air batteries. *Adv Sci* 2018;5:1700691. DOI PubMed PMC
165. Ge X, Sumboja A, Wuu D, et al. Oxygen reduction in alkaline media: from mechanisms to recent advances of catalysts. *ACS Catal* 2015;5:4643-67. DOI
166. Li X, Li C, Xie Y, Pan S, Luo F, Yang Z. Anion effect on oxygen reduction reaction activity of nitrogen doped carbon nanotube encapsulated cobalt nanoparticles. *Appl Surf Sci* 2024;648:158975. DOI
167. Zhu Y, Peng W, Li Y, Zhang G, Zhang F, Fan X. Modulating the electronic structure of single-atom catalysts on 2D nanomaterials for enhanced electrocatalytic performance. *Small Methods* 2019;3:1800438. DOI
168. Zhang J, Dong X, Xing W, et al. Engineering iron single atomic sites with adjacent ZrO_2 nanoclusters via ligand-assisted strategy for effective oxygen reduction reaction and high-performance Zn-air batteries. *Chem Eng J* 2021;420:129938. DOI
169. ul Haq M, Wu DH, Ajmal Z, et al. Derived-2D $Nb_4C_3T_x$ sheets with interfacial self-assembled Fe-N-C single-atom catalyst for electrocatalysis in water splitting and durable zinc-air battery. *Appl Catal B Environ Energy* 2024;344:123632. DOI
170. Xu X, Li X, Lu W, et al. Collective effect in a multicomponent ensemble combining single atoms and nanoparticles for efficient and durable oxygen reduction. *Angew Chem Int Ed* 2024;63:e202400765. DOI
171. Cao S, Chen H, Hu Y, et al. MXene-based single atom catalysts for efficient CO_2RR towards CO: a novel strategy for high-throughput catalyst design and screening. *Chem Eng J* 2023;461:141936. DOI
172. Tan X, Sun K, Zhuang Z, et al. Stabilizing copper by a reconstruction-resistant atomic Cu-O-Si interface for electrochemical CO_2 reduction. *J Am Chem Soc* ;2023:8656-64. DOI
173. Iqbal MS, Yao Z, Ruan Y, et al. Single-atom catalysts for electrochemical N_2 reduction to NH_3. *Rare Met* 2023;42:1075-97. DOI
174. Suryanto BHR, Du HL, Wang D, Chen J, Simonov AN, Macfarlane DR. Challenges and prospects in the catalysis of electroreduction of nitrogen to ammonia. *Nat Catal* 2019;2:290-6. DOI
175. Zhang M, Xu W, Ma CL, Yu J, Liu YT, Ding B. Highly active and selective electroreduction of N_2 by the catalysis of Ga single atoms stabilized on amorphous TiO_2 nanofibers. *ACS Nano* 2022;16:4186-96. DOI
176. Han Z, Tranca D, Rodríguez-Hernández F, et al. Embedding Ru clusters and single atoms into perovskite oxide boosts nitrogen fixation and affords ultrahigh ammonia yield rate. *Small* 2023;19:e2208102. DOI
177. Nguyen TP, Kim IT. Single-atom transition metal photocatalysts for hydrogen evolution reactions. *Catalysts* 2022;12:1304. DOI
178. Fauth C, Lenzer A, Abdel-Mageed AM, Jürgen Behm R. Temporal analysis of products (TAP) reactor study of the dynamics of CO_2 interaction with a Ru/γ-Al_2O_3 supported catalyst. *Appl Catal B Environ Energy* 2023;334:122817. DOI
179. Lin Z, Wang Y, Peng Z, et al. Single-metal atoms and ultra-small clusters manipulating charge carrier migration in polymeric perylene diimide for efficient photocatalytic oxygen production. *Adv Energy Mater* 2022;12:2200716. DOI

180. Ran J, Zhang J, Yu J, Jaroniec M, Qiao SZ. Earth-abundant cocatalysts for semiconductor-based photocatalytic water splitting. *Chem Soc Rev* 2014;43:7787-812. DOI
181. Akhundi A, Habibi-Yangjeh A, Abitorabi M, Rahim Pouran S. Review on photocatalytic conversion of carbon dioxide to value-added compounds and renewable fuels by graphitic carbon nitride-based photocatalysts. *Catal Rev* 2019;61:595-628. DOI
182. Xia B, Zhang Y, Shi B, Ran J, Davey K, Qiao S. Photocatalysts for hydrogen evolution coupled with production of value-added chemicals. *Small Methods* 2020;4:2000063. DOI
183. Tentu RD, Basu S. Photocatalytic water splitting for hydrogen production. *Curr Opin Electrochem* 2017;5:56-62. DOI
184. Chen X, Zhao J, Li G, Zhang D, Li H. Recent advances in photocatalytic renewable energy production. *Energy Mater* 2022;2:200001. DOI
185. Wang F, Yang S, Han S, et al. Synthesis of Cu-TiO_2/CuS pn heterojunction via in situ sulfidation for highly efficient photocatalytic NO removal. *Prog Nat Sci* 2022;32:561-9. DOI
186. Kerketta U, Kim H, Denisov N, Schmuki P. Grätzel-type TiO_2 anatase layers as host for pt single atoms: highly efficient and stable photocatalytic hydrogen production. *Adv Energy Mater* 2024;14:2302998. DOI
187. Lee BH, Park S, Kim M, et al. Reversible and cooperative photoactivation of single-atom Cu/TiO_2 photocatalysts. *Nat Mater* 2019;18:620-6. DOI
188. Chen Y, Qi M, Li Y, et al. Activating two-dimensional $Ti_3C_2T_x$-MXene with single-atom cobalt for efficient CO_2 photoreduction. *Cell Rep Phys Sci* 2021;2:100371. DOI
189. Xu Q, Wang L, Sheng X, et al. Understanding the synergistic mechanism of single atom Co-modified perovskite oxide for piezo-photocatalytic CO_2 reduction. *Appl Catal B Environ Energy* 2023;338:123058. DOI
190. Cao Y, Guo L, Dan M, et al. Modulating electron density of vacancy site by single Au atom for effective CO_2 photoreduction. *Nat Commun* 2021;12:1675. DOI PubMed PMC
191. Gao C, Low J, Long R, Kong T, Zhu J, Xiong Y. Heterogeneous single-atom photocatalysts: fundamentals and applications. *Chem Rev* 2020;120:12175-216. DOI
192. Li S, Li Y, Bai H, et al. Penta-coordinated aluminum species: anchoring Au single atoms for photocatalytic CO_2 reduction. *Appl Catal B Environ Energy* 2024;345:123703. DOI
193. Li SQ, Liu Y, Li YL, et al. Development of γ-Al_2O_3 with oxygen vacancies induced by amorphous structures for photocatalytic reduction of CO_2. *Chem Commun* 2022;58:11649-52. DOI
194. Zhao Z, Xiao D, Chen K, et al. Nature of five-coordinated Al in γ-Al_2O_3 revealed by ultra-high-field solid-state NMR. *ACS Cent Sci* 2022;8:795-803. DOI PubMed PMC
195. Martin O, Martín AJ, Mondelli C, et al. Indium oxide as a superior catalyst for methanol synthesis by CO_2 hydrogenation. *Angew Chem Int Ed* 2016;55:6261-5. DOI
196. Zhao H, Yu R, Ma S, et al. The role of Cu_1-O_3 species in single-atom Cu/ZrO_2 catalyst for CO_2 hydrogenation. *Nat Catal* 2022;5:818-31. DOI
197. Wu C, Lin L, Liu J, et al. Inverse ZrO_2/Cu as a highly efficient methanol synthesis catalyst from CO_2 hydrogenation. *Nat Commun* 2020;11:5767. DOI PubMed PMC
198. Zhou H, Chen Z, López AV, et al. Engineering the Cu/Mo_2CT_x (MXene) interface to drive CO_2 hydrogenation to methanol. *Nat Catal* 2021;4:860-71. DOI